DMD Fast Forward. Published on May 5, 2021 as DOI: 10.1124/dmd.120.000349
This article has not been copyedited and formatted. The final version may differ from this version.

Title Page

Evaluation of the Absorption, Metabolism, and Excretion of a Single Oral 1 mg Dose of Tropifexor in Healthy Male Subjects and the Concentration Dependency of Tropifexor Metabolism

*Lydia Wang-Lakshman, Zhuang Miao, Lai Wang, Helen Gu, Mark Kagan, Jessie Gu, Elizabeth McNamara, Markus Walles, Ralph Woessner, Gian Camenisch, Heidi J. Einolf, Jin Chen

Novartis Institute for Biomedical Research, East Hanover, United States (LW-L., ZM, LW, HG, MK, HJE, JC); Novartis Institute for BioMedical Research, Cambridge, United States (JG, EM); Novartis Institute for Biomedical Research Basel, Switzerland (MW, RW, GC)

DMD Fast Forward. Published on May 5, 2021 as DOI: 10.1124/dmd.120.000349
This article has not been copyedited and formatted. The final version may differ from this version.

Running Title Page

Running title: Metabolic pathways and disposition of Tropifexor in humans

Corresponding author: *Ms. Lydia Wang-Lakshman; One Health Plaza, East Hanover, NJ 07936-1080; Lydia.wang@novartis.com.

Number of text pages: 46

Number of tables: 9

Number of figures: 8

Number of references: 21

Number of words in Abstract: 237

Number of words in Introduction: 715

Number of words in Discussion: 1535

A list of nonstandard abbreviations: AME, absorption, metabolism and excretion, AUC_{last}, area under the plasma concentration-time curve from time zero to time of last measurable concentration; AUC_{inf}, area under the plasma concentration-time curve from time zero to infinity; BA, bile acid; BSEP, bile salt export pump; Ci, curie; CL/F, clearance unadjusted for the bioavailable; CL_{int}, intrinsic clearance; CL_H , hepatic clearance;

C_{max}, the maximum exposure; CYP, cytochrome P450; FGF, fibroblast growth factor; FXR, farnesoid X receptor; HH, human hepatocyte; HLM, human liver microsome; HPLC, high performance liquid chromatography; LC-MS/MS, liquid chromatography with tandem mass spectroscopy; LSC, liquid scintillation counting; MBq, megabecquerel;

NASH, non-alcoholic steatohepatitis; PD, pharmacodynamics; PK, pharmacokinetics;

DMD Fast Forward. Published on May 5, 2021 as DOI: 10.1124/dmd.120.000349
This article has not been copyedited and formatted. The final version may differ from this version.

OCA, obeticholic acid; rhCYP, recombinant human CYP; rhUGT, recombinant human UGT; SHP, small heterodimer partner; $T_{1/2}$, half-life; T_{max}, time to reach C_{max}; UDPGA, UDP glucoronic acid; UGT, UDP-glucuronosyltransferase; UPLC, ultra-performance liquid chromatography; V_z/F, estimation volume of distribution unadjusted for the bioavailable.

DMD Fast Forward. Published on May 5, 2021 as DOI: 10.1124/dmd.120.000349
This article has not been copyedited and formatted. The final version may differ from this version.

Abstract

Tropifexor (NVP-LJN452) is a highly potent, selective, non-steroidal, non-bile acid farnesoid X receptor (FXR) agonist for the treatment of nonalcoholic steatohepatitis (NASH). Its absorption, metabolism, and excretion were studied following a 1-mg oral dose of [^{14}C]tropifexor to four healthy male subjects. Mass balance was achieved with ~94% of the administered dose recovered in excreta through 312 hours collection period. Fecal excretion of tropifexor-related radioactivity played a major role (~65% of the total dose). Tropifexor reached a maximum blood concentration (C_{max}) of 33.5 ng/mL with a median T_{max} of 4 hours and was eliminated with a plasma elimination half-life ($T_{1/2}$) of 13.5 hours. Unchanged tropifexor was the principal drug-related component found in plasma (~92% of total radioactivity). Two minor oxidative metabolites, M11.6 and M22.4, were observed in circulation. Tropifexor was eliminated predominantly via metabolism with >68% of the dose recovered as metabolites in excreta. Oxidative metabolism appeared to be the major clearance pathway of tropifexor. Metabolites containing multiple oxidative modifications and combined oxidation and glucuronidation were also observed in human excreta. The involvement of direct glucuronidation could not be ruled out, based on previous in vitro and nonclinical in vivo studies indicating its contribution to tropifexor clearance. The relative contribution of the oxidation and glucuronidation pathways appeared to be dose-dependent upon further in vitro investigation. Due to these complexities and the instability of glucuronide metabolites in the gastrointestinal tract, the contribution of glucuronidation remained undefined in this study.

Significance statement

Tropifexor was found to be primarily cleared from human body via oxidative metabolism. In vitro metabolism experiments revealed that the relative contribution of oxidation and glucuronidation was concentration-dependent with glucuronidation as the predominant pathway at higher concentrations while oxidative process becoming more important at lower concentrations near clinical exposure range. The body of work demonstrated the importance of carefully designed in vivo and in vitro experiments for better understanding of disposition processes during drug development.

DMD Fast Forward. Published on May 5, 2021 as DOI: 10.1124/dmd.120.000349
This article has not been copyedited and formatted. The final version may differ from this version.

Introduction

The farnesoid X receptor (FXR) is a bile acid (BA)-activated nuclear receptor, expressed predominantly in the liver, kidney, intestine, and adrenals (Parks et al., 1999). In the liver, the FXR is expressed primarily in parenchymal cells and to a lesser extent in Kupffer cells and stellate cells. It acts as a sensor of elevated BA levels (Meadows et al., 2020) and initiates homeostatic responses to control BA levels and modulate other metabolic processes such as gluconeogenesis and lipogenesis (Schaap et al., 2014). Elevated BA level is associated with inflammation and tumorigenesis, the diverse pathogeneses which are involved in different liver diseases (Zhu et al., 2016). Activation of the FXR reduces BA synthesis by increasing expression of BA transporters and modulating lipoprotein metabolism (Meadows et al., 2020). It also increases glucose disposal (even in type 2 diabetic patients) decreases lipogenesis-associated inflammation and reduces fibrosis (Ratziu et al., 2019). Thus, activation of the FXR is proposed to be an effective treatment option for different liver diseases associated with BA dysregulation, such as intrahepatic cholestasis, non-alcoholic steatohepatitis (NASH), and BA malabsorption diarrhea (Schaap et al., 2014; Walters et al., 2015).

Activation of the FXR in the liver upregulates the small heterodimer partner (SHP) signaling cascade. This inhibits the transcription of CYP7A1 and CYP8B1 genes (Schaap et al. 2014; Chiang 2015; Tully et al 2017; Chiang 2017; Chiang and Ferrell 2018) and activates the mitogen-activated protein kinase (MAPK) signaling pathway via inducing FGF-19 leading to downregulation of CYP7A1 and subsequent inhibition of BA synthesis (Schaap et al. 2014; Tully et al. 2017; Chiang and Ferrell 2018). Activation of

DMD Fast Forward. Published on May 5, 2021 as DOI: 10.1124/dmd.120.000349
This article has not been copyedited and formatted. The final version may differ from this version.

the FXR-SHP cascade is also associated with anti-inflammatory, antifibrotic, and anticholestatic effects (Calkin and Tontonoz, 2012; Schaap et al. 2014).

Several FXR agonists are in clinical development for the treatment of NASH and hepatic fibrosis. Among them, obeticholic acid (OCA; 25 mg), a BA FXR agonist, was shown to improve fibrosis and histological features of NASH in a multicenter, randomized, placebo-controlled phase 3 clinical trial (Younossi et al., 2019). Although OCA demonstrated favorable results in treating NASH, a high rate of pruritus and adverse effect on the lipid profile (increase in total cholesterol and low-density lipoprotein cholesterol) were observed in OCA-treated versus placebo-treated patients (Neuschwander-Tetro et al., 2015; Polyzos et al., 2020).

To address these limitations, the development of a novel FXR agonists with improved efficacy, safety and tolerability than the current standard is necessary. Tully et al. (2017) discovered tropifexor, a highly potent non-BA FXR agonist. Tropifexor has been shown to induce FXR target genes (SHP, BSEP, CYP8B1 and FGF 15) at very low doses and to provide systematic FXR exposure in rodents (Tully et al., 2017). In the liver, inductions of SHP, BSEP, and CYP8B1 were observed at tropifexor doses of 0.01 mg/kg, 0.003 mg/kg, and 0.03 mg/kg, respectively. In the ileum, SHP and FGF15 were induced at doses as low as 0.01 mg/kg. In addition, plasma FGF15 protein concentration came down to the baseline at 24 hours following the final dose, suggesting that tropifexor administration does not lead to prolonged exposure to FXR activation (Tully et al., 2017).

In the preclinical NASH model, tropifexor showed marked reduction in steatohepatitis, fibrosis and pro-fibrogenic gene expression. The efficacy of tropifexor (at <1 mg/kg) was

DMD Fast Forward. Published on May 5, 2021 as DOI: 10.1124/dmd.120.000349
This article has not been copyedited and formatted. The final version may differ from this version.

found to be superior to that of OCA (at 25 mg/kg) in the liver of insulin-resistant obese amylin liver NASH model (AMLN) mice (Hernandez et al., 2019). In the first-in-human study, tropifexor (single ascending dose: 0.01 to 3 mg; multiple ascending dose: 0.01-0.1 mg once daily for 14 days) was well tolerated in healthy volunteers with an acceptable safety profile. The pharmacokinetic (PK) profile was also found to be suitable for once-daily dosing (Badman et al., 2020).

Our study investigated the absorption, metabolism and excretion (AME) of tropifexor in healthy humans. The rates and routes of excretion of [^{14}C]tropifexor-related radioactivity were determined, including the mass balance of total drug-related radioactivity in excreta. Key biotransformation pathways and clearance mechanisms were elucidated in the study. To gain a better understanding of the disposition behavior of tropifexor in humans, additional in vitro studies were conducted to identify and characterize enzymes involved in the metabolism of tropifexor, assess the relative contributions of the different biotransformation pathways to total tropifexor metabolism; as well as evaluating the potential for concentration-dependent metabolism.

Materials and Methods

Human study

Study drug for clinical trial

Radiolabeled [^{14}C]tropifexor for the clinical study was supplied as free form bulk dose container ([^{14}C]tropifexor powder in bottle) by Novartis authorized contract manufacturing organization (Pharmaron, Inc.). When reconstituted and dispensed, the dosage form was an oral solution containing 1 mg [^{14}C]tropifexor (free form) with a

DMD Fast Forward. Published on May 5, 2021 as DOI: 10.1124/dmd.120.000349
This article has not been copyedited and formatted. The final version may differ from this version.

corresponding 60 µCi (2.22 MBq) radioactivity. Radiochemical purity of ^{14}C labeled drug substances for human study was ≥98%. Figure 1 illustrates the chemical structure, molecular formula, and specific radioactivity of [^{14}C]tropifexor.

Study design

The human absorption, metabolism and excretion (AME) study was an open-label, single-dose study conducted in four healthy male subjects aged between 18 to 45 years with a body mass index (BMI) of 18 to 30 $kg \cdot m^{-2}$. The clinical study protocol was reviewed by the Institutional Review Board (IRB), and the study was conducted according to the ethical principles of the 1964 Declaration of Helsinki and its later amendments. Informed consent was obtained from each subject in writing before enrollment.

Subjects were restricted to the clinical research unit (Covance, Madison, WI, USA) under observation for around 24 hours before drug administration. Following overnight fasting of 10 hours, the four qualified subjects received a single, oral 1 mg dose of [^{14}C]tropifexor (60 µCi). Recovery of radioactivity in excreta from each subject was monitored daily during the study. Subjects remained domiciled for a period of at least 7 days. From day 7-13, subjects were discharged if the cumulative recovery of radioactivity in excreta was ≥90% and the combined urinary and fecal excretion was ≤1% of the administered dose per 24 hours for 2 consecutive days. All subjects were released in the morning of day 14 irrespective of radioactivity recovery. Blood and plasma samples for PK, total radioactivity, and metabolite analysis were collected before administration of the dose and at 1, 2, 3, 4, 6, 8, 12, 24, 48, 72, 96, 120, 144, 168, 192, 216, 240, 264, 288, and 312 hours post-dose. Each sample was collected into

DMD Fast Forward. Published on May 5, 2021 as DOI: 10.1124/dmd.120.000349
This article has not been copyedited and formatted. The final version may differ from this version.

a pre-cooled tube containing the anticoagulant, K_2EDTA. Plasma samples were centrifuged, and the supernatants were isolated. Urine samples were collected at 0-6, 6-12 and 12-24 hours, and in 24-hours intervals thereafter until release. Feces samples were collected as passed from the hour of dosing until release. All samples were stored at −70°±10°C until analysis.

Determination of total radioactivity in human blood, plasma, urine, and feces

Investigation of total radioactivity in human blood, plasma, urine and feces was performed by Covance Laboratories (Madison, WI, USA) using liquid scintillation counting (LSC). Plasma and urine samples were analyzed by direct LSC after homogenizing each sample. Duplicate or triplicate aliquots were mixed with a scintillation cocktail before analyzing in a Packard liquid scintillation counter (Perkin Elmer Corporation, Waltham, MA, USA). Blood samples were aliquoted and combusted in a Model 307 Sample Oxidizer (Packard Instrument Company Inc., Meriden, CT, USA). The resulting $^{14}CO_2$, captured in Carbo-Sorb (Perkin Elmer Corporation, Waltham, MA, USA), was analyzed using LSC after mixing with Permafluor (Perkin Elmer Corporation, Waltham, MA, USA). All samples were aliquoted utilizing gravimetric measurement. Feces samples were combined at 24-hour intervals for each subject and weighed. A measured amount of water (approximately 2-3 times of the sample weight) was added and the sample was homogenized. Triplicate aliquots of fecal homogenate (roughly 0.2 g) were combusted and analyzed by LSC.

A conversion factor of 1 µCi per 2.22×10^6 dpm was used to convert radioactivity from dpm to µCi. For blood and plasma, the radioactivity was converted to a concentration of

DMD Fast Forward. Published on May 5, 2021 as DOI: 10.1124/dmd.120.000349
This article has not been copyedited and formatted. The final version may differ from this version.

drug related material (ng-eq/g or pmol/mL) using the aliquot weight and the specific activity of the drug (35.7μCi/μmol or 59 μCi/mg). For urine and feces samples, the measured radioactivity was converted to a percentage of dose recovery using the aliquot weight, the total weight of the collected sample, and the known radioactivity of the dose. To determine the mass-balance, the cumulative percentage dose recovered from all of the collected urine and feces were calculated.

Pharmacokinetic analysis

Tropifexor concentration in plasma was determined using a validated liquid chromatography-tandem mass spectrometry (LC-MS/MS) method. The C_{max}, T_{max}, AUC_{last}, AUC_{inf}, $T_{1/2}$, V_z/F and CL/F were determined for tropifexor concentrations in plasma and C_{max}, T_{max}, AUC_{last} and AUC_{inf} were determined for the total radioactivity measurements of [^{14}C]tropifexor in plasma and the whole blood. As aliquots of blood and plasma were weighed for total radioactivity analysis, results in ng-eq/g were converted to ng-eq/mL using a conversion factor of 1 g = 1 mL. The PK parameters were determined by applying non-compartmental methods using Phoenix WinNonlin software, Certara, Princeton, NJ, USA.

Sample preparation for metabolite analysis

Plasma

For metabolite assessment, equal volume aliquots of plasma samples were pooled across the four subjects at pre-dose and at selected time-points post-dose. Pooled plasma samples (~4 mL) were then processed for analysis by protein precipitation using measured ratio of appropriate organic solvents. Following vortex mixing, samples were centrifuged at 5580 × g for 10 minutes at 10°C and the supernatants were collected.

The organic portions of the supernatants were evaporated under a stream of nitrogen and the resulting sample was frozen. The frozen sample was lyophilized to dryness and the residue was subsequently reconstituted with aqueous and organic solvents at appropriate ratios to obtain a ~20-fold concentration of the original sample.

Urine

A urine sample pool, representing >91% of the excreted radioactivity in urine, was prepared for each subject by taking equal percentages of volume excreted from each collection interval. An aliquot of the pooled urine sample was frozen and subsequently lyophilized to dryness. The resulting residue was reconstituted to one-tenth of the original volume with mobile phase A (5 mM ammonium formate with 0.1% formic acid) for LC-MS/MS analysis.

Feces

A cumulative fecal homogenate pool, representing >92% of the excreted radioactivity in feces, was prepared for each subject by taking an equal percentage (by weight) of the excreted sample in each 24-hour interval. In addition to the cumulative pool, some individual fecal samples at later time points, when the absorption process was likely to be completed, were also analyzed to evaluate the relative level of intact tropifexor in these samples. Aliquots of the pooled and selected individual fecal homogenate samples from each subject were extracted multiple times with appropriate organic solvents. After each extraction, the supernatants of the extract were collected by centrifugation and combined. The organic portions of the extract were evaporated under a stream of nitrogen and the remaining aqueous part was frozen and lyophilized. Residue was reconstituted with mobile phase A (5 mM ammonium formate with 0.1%

DMD Fast Forward. Published on May 5, 2021 as DOI: 10.1124/dmd.120.000349
This article has not been copyedited and formatted. The final version may differ from this version.

formic acid): B (acetonitrile with 0.1% formic acid) in a 9:1 (v/v) ratio. The samples were further centrifuged to remove any particulate. The clear supernatant was analyzed for tropifexor and metabolites using LC-MS. The final reconstituted sample represented 10-fold concentration from the fecal homogenate.

Liquid chromatography and mass spectrometry analysis of metabolites

Chromatographic separation of tropifexor and its metabolites was performed using Acquity ultra-performance liquid chromatography (UPLC) systems (Waters, Milford, MA) equipped with a Mac-Mod ACE Excel 2 AQ UPLC column (3 mm × 150 mm, 2.1 µm particle size, Mac-Mod, Chadds Ford, PA). The column was maintained at 35°C and the elution was achieved with a flow rate of 0.5 mL/min. The mobile phases consisted of solvent A (5 mM ammonium formate with 0.1% formic acid) and solvent B (acetonitrile with 0.1% formic acid). A linear gradient elution was used. The linear elution gradient started at 10% B and increased to 90% B by 30 min, maintained at 90% B for 10 min, decreased to 10% B from 40-41 min, then finally held at 10% B from 41-50 min. The LC eluent was split at 1:10 volume ratios with one part directed to the mass spectrometer and 10 parts for radioactivity detection (see Supplementary Appendix).

Structural elucidation of the metabolites was carried out using the LTQ Orbitrap Elite mass spectrometer (Thermo Fisher Scientific, Waltham, MA, USA) interfaced with Acquity UPLC systems (Waters, Milford, MA, USA). Source parameters were adjusted to optimize analyte response in the positive electrospray ionization (+ESI) mode for the MS system. Full scan MS spectra were typically obtained in profile mode while product ion (MS/MS) spectra were generated in centroid mode using either data-dependent

DMD Fast Forward. Published on May 5, 2021 as DOI: 10.1124/dmd.120.000349
This article has not been copyedited and formatted. The final version may differ from this version.

acquisition (DDA) MS/MS or dedicated MS/MS scans. The analytes were fragmented using high-energy collisional dissociation (HCD) of the molecular ion. Metabolite structural elucidation and assignment were based on their HPLC retention times, full scan accurate MS spectral analysis with exact mass confirmation against theoretical elemental composition, and product ion (MS/MS) mass spectra.

Quantitative assessment of tropifexor and metabolites

During LC-MS/MS analyses of samples for metabolite profiling, the majority of the LC eluent (10 parts) was collected via an HTC Collect PAL fraction collector (Leap Technologies, Carrboro, NC) into 96-well Luma plates for off-line radiochromatographic profiling. Luma plates were dried and subsequently counted on a TopCount NXT (Perkin Elmer, Shelton, CT, USA). Laura software (LabLogic System Ltd., Sheffield, UK) was used for data processing and generation of radiochromatograms. The concentration or amount of each component peak was calculated as its fraction of radioactivity in a particular peak multiplied by the total concentration (ng-eq/g) in plasma or the percentage of the dose in the excreta. Metabolite concentrations were reported in ng-eq/mL. Details are provided in the Supplementary Appendix.

DMD Fast Forward. Published on May 5, 2021 as DOI: 10.1124/dmd.120.000349
This article has not been copyedited and formatted. The final version may differ from this version.

In vitro studies

Chemicals, reagents, and standards

Pooled human liver microsomes (HLM) (lot 38289, n = 150 donors, mixed gender) were purchased from Corning Gentest (Tewksbury, MA, USA). Microsomal preparations from baculovirus-infected insect cells expressing individual recombinant human (rh) CYP or rhUGT enzymes, control microsomes, and NADPH regenerating system were also purchased from Corning Gentest (Tewksbury, MA, USA). LiverPool^{TM} 20-donor mixed gender pooled cryopreserved human hepatocytes (lot OAP), InVitroGRO KHB (a modified Krebs-Henseleit buffer for hepatocyte incubation) and InVitroGRO Thawing Medium (HT) were purchased from BioreclamationIVT (Baltimore, MD). Fetal bovine serum (FBS) was purchased from Invitrogen (Walkersville, MD). FBS (100%) was added to KHB to make 2% (v/v) FBS in KHB. Ammonium formate (10 mM) was purchased from Hampton Research (Aliso Viejo, CA). [^{14}C]tropifexor (specific activity of 42.4 or 53.3 mCi/mmol with radiochemical purity of >98%) and stable labeled [M+5]tropifexor was obtained from Novartis Isotope Laboratory (East Hanover, NJ). FlowLogic U was purchased from LabLogic System, Inc. (Brandon, FL, USA). Opti-Fluor was from PerkinElmer Life and Analytical Sciences (Boston, MA, USA). All other chemicals and solvents were of analytical grade and were obtained from commercial sources.

In vitro hepatic metabolism of tropifexor and relative contributions of individual CYP or UGT enzymes to metabolic clearance

The methods for in vitro metabolism of tropifexor in HLM and human hepatocytes (HH) including estimations of the relative contributions of individual CYP or UGT enzymes to

DMD Fast Forward. Published on May 5, 2021 as DOI: 10.1124/dmd.120.000349
This article has not been copyedited and formatted. The final version may differ from this version.

tropifexor hepatic metabolic clearance by oxidation or glucuronidation can be found in the Supplementary Appendix.

Estimation of fractional metabolism by CYP and UGT in human hepatocytes and dose dependency

The relative contribution of CYP and UGT metabolism to total tropifexor metabolic clearance (and its dose dependency) in HH in vitro was determined by selective chemical inhibitors for each metabolic pathway using different tropifexor concentrations (method described later). In addition, relative contributions of these enzyme pathways to total tropifexor metabolism were evaluated by measuring the rate of specific metabolite formation in HH using different tropifexor concentrations (method described in the Supplementary Appendix).

To evaluate the contributions of CYP and UGT to the overall metabolism of tropifexor in HH using chemical inhibition, the CL_{int} of tropifexor with 1-aminobenzotriazole (3 uM ABT, CYP inhibitor), or 0.5 uM borneol (UGT inhibitor) (Jinno et al., 2014) and/or 0.05 uM ATZ (inhibitor of UGT1A1/3) (Zhang et al., 2005) was determined and compared to the CL_{int} without inhibitors. Cryopreserved hepatocytes were processed as described by the supplier (described in the Supplementary Appendix). Five hundred microliters (~10^6 cells) of the final cell suspension were added to triplicate wells of a 12-well plate pre-dispensed with 0.5 mL of KHB and tropifexor (0.005 or 0.1 µM, nominal concentration) with different inhibitors. Control wells contained no inhibitor. The plate was incubated at 37°C in a humidified cell culture incubator (5% CO2, 95% air) without shaking for 0, 0.5, 1, 2, 3, and 4 hours. At each time point, an aliquot (150 µL) of each incubation mixture was removed and quenched

with an equal volume of cold acetonitrile with 30 ng/mL of internal standard. The precipitated pellet was removed by centrifugation and an aliquot of each sample was analyzed using the LC-MS/MS MRM method. Clearance calculations and estimation of relative contributions of CYP and UGT enzymes to tropifexor metabolism can be found in the Supplementary Appendix.

DMD Fast Forward. Published on May 5, 2021 as DOI: 10.1124/dmd.120.000349
This article has not been copyedited and formatted. The final version may differ from this version.

Results

A single oral dose of 1 mg [^{14}C]tropifexor was well tolerated in healthy male subjects. No serious adverse events (AEs) or severe AEs were reported during the study. All four subjects completed the study.

Pharmacokinetics parameters and total radioactivity of tropifexor in plasma

Following a 1mg oral dose of [^{14}C]tropifexor in human, plasma concentrations of both tropifexor and total radioactivity increased to mean peak levels of 33.5 (± 5.74) ng/mL and 37.9 (±7.24) ng-eq/g, respectively, with a median T_{max} of 4 hours (Table 1). Thereafter, the plasma concentrations decreased with a mean elimination half-life of 13.5 (±2.04) hours for tropifexor and 20.4 (±4.49) hours for total radioactivity. Quantifiable concentrations of plasma tropifexor were observed for up to 120 hours post-dose, while plasma total radioactivity concentrations were quantifiable for up to 96 hours post-dose (Figure 2). The mean plasma exposure of the tropifexor parent compound (AUC_{inf} = 553 h*ng/mL) accounted for ~82% of the total plasma radioactivity exposure (AUC_{inf} = 674 h*ng-eq/g), indicating tropifexor as the major circulating component. The intersubject variability associated with C_{max} and AUC_{inf} for tropifexor and total radioactivity were ranging from 17-20%.

Mass balance and excretion of tropifexor in humans

Adequate mass balance was achieved following a single oral dose of [^{14}C]tropifexor to healthy human subjects. The cumulative recovery of radioactivity from human subjects through the last collection time point (312 hours) was an average of 93.8% (±4.29%). The radioactive dose was excreted in both feces and urine with fecal excretion playing a

DMD Fast Forward. Published on May 5, 2021 as DOI: 10.1124/dmd.120.000349
This article has not been copyedited and formatted. The final version may differ from this version.

relatively more important role. The mean urinary excretion was 28.5% (±2.79%), while the mean fecal excretion was 65.3% (±4.12%). The excretion of radioactivity was rapid, with the majority of the dose excreted within 96 hours post-dose in both urine and feces (Figure 3).

Tropifexor metabolism in humans

Metabolite profiles in plasma

The representative tropifexor metabolite profiles in circulation at T_{max} and 24 hours post-dose are provided in Figure 4. Plasma radioactivity was quantifiable up to 72 hours post-dose using radiometric profiling; thus, calculations of metabolite and tropifexor exposure were based on total radioactivity exposure up to 72 hours post-dose ($AUC_{0\text{-}72h}$ = 629 ng-eq/mL). The most prominent drug-related component in the plasma was tropifexor, accounting for ~91.6% of total radioactivity $AUC_{0\text{-}72h}$. Two minor circulating metabolites were observed. The *O*-dealkylation metabolite M11.6 accounted for ~1.7% of the total radioactivity $AUC_{0\text{-}72h}$, while the mono-oxy metabolite M22.4 accounted for 5.0% of the total radioactivity $AUC_{0\text{-}72h}$. Plasma concentrations and PK parameters of tropifexor and its metabolites in circulation are presented in Table 2.

Metabolite profiles in excreta

The metabolites observed in human excreta are expressed as a percentage of the administered dose (Table 3). Representative radiochromatograms showing metabolite profiles in human urine and feces are illustrated in Figure 5. Metabolites observed in human urine were mainly results of oxidative *O*-dealkylation and further glucuronidation or oxidation. The main metabolite observed in the urine was M8.8, a metabolite

DMD Fast Forward. Published on May 5, 2021 as DOI: 10.1124/dmd.120.000349
This article has not been copyedited and formatted. The final version may differ from this version.

combining glucuronidation and *O*-dealkylation, accounting for 10.8% of the dose on average. O-dealkylation of tropifexor led to two stereoiosmers, M10.8 and M11.6, accounting for 3.7% and 4.9% of the dose in urine, respectively. Two other metabolites were observed at lower levels and included M6 (combination of mono-oxidation and *O*-dealkylation) and M6.7 (glucuronide of *O*-dealkylation). Tropifexor was not observed in the urine.

In contrast, intact tropifexor was the main component in feces, as an average of 25.4% (±4.67) of the dose. Metabolites observed in feces were as a result of oxidative metabolism. The main metabolite observed in feces was M6, a mono-oxidation of the *O*-dealkylation metabolite, accounting for 8.6% of the dose. M10.8 and M11.6 accounted for 3.3% and 6.5% of the dose, respectively. Mono-oxidation of tropifexor resulted in M24 (2.6% of the dose) and M22.4. M22.4 co-eluted with a di-oxidation metabolite, M19.5. The sum of the two contributed to a total of ~8.0% of the dose. Other minor metabolites observed in human feces included M18.1 and M18.2, each accounting for 2-3% of the dose. Several minor peaks were observed in the urine and feces, but were un-identifiable, each contributing to <2% of the total dose. Accurate mass of the acyl-glucuronide metabolite, M22 (m/z 782.1877), with 5 ppm tolerance was extracted from full scan mass spectra of both urine and feces samples. However, no discernable peak was observed in human excreta, confirming the absence of M22.

Estimation of tropifexor absorption in human

The fraction of the dose absorbed (F_a) was calculated as the sum of the fraction of the dose excreted in the urine (F_{urine}) and the fraction of dose excreted as metabolites in feces ($F_{metabolite\ in\ feces}$) as in the following equation:

DMD Fast Forward. Published on May 5, 2021 as DOI: 10.1124/dmd.120.000349
This article has not been copyedited and formatted. The final version may differ from this version.

$$Fa = F_{urine} + F_{metabolites\ in\ feces}$$ ..... Eq. 1

Average absorption, estimated based on this equation, was 68.4% (range 63.0-71.8%) in human subjects. This estimation assumes the amount of intact tropifexor in the feces is entirely unabsorbed dose. In cases where the absorbed parent was metabolized to direct glucuronides and subsequently hydrolyzed back to the parent in the GI tract, or the intact parent was absorbed and eliminated via direct intestinal or biliary excretion, the F_a would be better estimated by adding back the contribution from the aforementioned processes:

$$Fa = F_{urine} + F_{metabolite\ in\ feces} + F_{absorbed\ parent\ in\ feces}$$ .....Eq. 2

where $F_{absorbed\ parent\ in\ feces}$ is the fraction of dose absorbed but appeared as the intact parent in feces. The $F_{absorbed\ parent\ in\ feces}$ was estimated from the late fecal profiles where absorption was assumed to be completed and the intact parent observed was presumably the result of unstable metabolites or the excreted parent (Figure 5C). We can also assume that the ratios of the absorbed parent-to-metabolite maintain constant over time in the feces, that is:

$$\frac{F_{absorbed\ parent\ in\ feces}}{F_{metabolite\ in\ feces}} = \frac{F_{absorbed\ parent\ in\ late\ fecal\ profile}}{F_{metabolite\ in\ late\ fecal\ profile}}$$

Eq. 3

The $F_{absorbed\ parent\ in\ feces}$ can then be estimated as follows:

$$F_{absorbed\ parent\ in\ feces} = \frac{F_{parent\ in\ late\ fecal\ profile}}{F_{metabolite\ in\ late\ fecal\ profile}} \times F_{metabolite\ in\ feces}$$ ....Eq. 4

Using these equations and assumptions, the fraction of the dose absorbed but appeared as the intact parent in feces was calculated to be ~7.5% (± 1.6%) based on

the late timepoint fecal profile. Therefore, the overall tropifexor absorption was calculated to be 75.9% (± 5.1%) on average.

Biotransformation pathways of tropifexor in human

Structural assignments of metabolites in humans, carried out by LC-MS/MS analysis with off-line radioactivity detection, were based on their relative HPLC retention times, full scan MS spectral analysis with exact mass confirmation against theoretical elemental composition, and product ion mass spectra. All metabolites observed in the human AME study with their accurate mass data, the proposed structure and fragmentation assignments are listed in Table 4. Metabolites detected at trace levels in human plasma by MS only were included and are noted as such. Product ion mass spectra of the parent and metabolites can be found in Supplementary Appendix (Figure SA02).

Based on metabolites characterized in human plasma and excreta, the overall biotransformation pathways of tropifexor are proposed and summarized in Figure 6. Overall, tropifexor appeared to be primarily metabolized via phase I oxidative pathways as the majority of radioactivity observed in human excreta consisted of oxidative metabolites. The primary oxidative pathways included oxidative O-dealkylation, and oxidation at the phenyl cyclopropyl isoxazole moiety and/or at the benzothiazole and fused ring structure. Metabolites containing multiple oxidative modifications and/or glucuronidation to oxidative products were also observed. The extent of the contribution from oxidative pathways to total tropifexor metabolism was estimated to be 68.4% (sum of all metabolites containing oxidative modification in excreta) of the dose. No quantifiable direct glucuronide metabolites were detected in humans in vivo.

DMD Fast Forward. Published on May 5, 2021 as DOI: 10.1124/dmd.120.000349
This article has not been copyedited and formatted. The final version may differ from this version.

Tropifexor metabolism in vitro

Tropifexor metabolism in HLM and HH

In incubations of [^{14}C]tropifexor (10 uM) with HLM, low levels of oxidative metabolites were formed (M11.6 and M22.4) in the presence of the CYP enzyme cofactor, NADPH. In the presence of both cofactors for CYP- and UGT-mediated metabolism, a predominance of the acyl-glucuronide (M22) was observed in the incubations (Supplementary Appendix, Figure SA01). In HH, at this same [^{14}C]tropifexor concentration, the predominance of the M22 acyl-glucuronide was also observed, in addition to a small proportion of the oxidative metabolites, M10.8 and M11.6 (data not shown). Representative product ion spectra of oxidative and acyl-glucuronide metabolites observed from in vitro incubations can be found in Supplementary Appendix (Figure SA03) and were comparable to those observed in human AME study.

Identity and relative contribution of CYP enzymes to the oxidative metabolism of tropifexor in the human liver

Among the rhCYP enzymes tested, appreciable metabolite formation above the control level was detectable in incubations with CYP1A1, CYP2C8, CYP2C9, and CYP3A4. Of particular note, the primary metabolite M11.6 was found to be formed by CYP3A4, M24 was formed by CYP2C9, and M22.4 by CYP2C8.

The contributions of different CYP enzymes to the oxidative metabolism of tropifexor were estimated based on the ability of selective inhibitors of specific CYP enzymes to inhibit total oxidative metabolism of tropifexor in HLM. Tropifexor clearance in HLM with or without selective inhibition were compared and corrected with the reported inhibitor cross-reactivity for individual CYP enzymes and normalized to 100%. In HLM, selective

inhibitors of CYP2C8 (montelukast), CYP2C9 (sulfaphenazole), or CYP3A (ketoconazole) inhibited total tropifexor metabolism by ~35%, 6.1%, or 74%, respectively. These three inhibitors were selected based upon the results of the rhCYP metabolism screening experiment, where these CYP enzymes were most active for tropifexor hepatic metabolism. After applying the correction and normalization, the relative contribution of CYP2C8, CYP2C9, and CYP3A to total tropifexor metabolism was estimated to be 15%, <0.1%, and 85%, respectively (Table 5). These data indicated that tropifexor hepatic microsomal oxidative metabolism is mainly due to CYP3A.

Additionally, the relative contributions of CYP3A and CYP2C8 to the total oxidative metabolism of tropifexor in the human liver was estimated using rhCYP kinetics and scaling the rhCYP $CL_{int,u}$ to the HLM $CL_{int,u}$ using a RAF (relative activity factor: the ratio of a specific CYP activity in the recombinant expressed microsomes versus the same specific CYP activity in the pooled HLM under substrate saturating conditions). The scaled CYP2C8 and CYP3A HLM CL_{int} was estimated to be 5.30 and 94.3 mL/h/mg microsomal protein, respectively (Table 6). This corresponded to a relative contribution of CYP2C8 and CYP3A to total tropifexor oxidative hepatic metabolism of approximately 5% and 95%, respectively. From the two methods described (chemical inhibition and rhCYP kinetics with scaling) it can be concluded that that the majority of tropifexor oxidative clearance is mediated by CYP3A4 (85-95%) with a minor contribution by CYP2C8 (5-15%) and negligible contribution by CYP2C9.

DMD Fast Forward. Published on May 5, 2021 as DOI: 10.1124/dmd.120.000349
This article has not been copyedited and formatted. The final version may differ from this version.

Identity and relative contributions of individual UGT enzymes to the total glucuronidation of tropifexor in the human liver

Appreciable tropifexor metabolism above control levels was detectable in incubations with the rhUGT1A1, rhUGT1A3, rhUGT1A7, and rhUGT1A9 enzymes, leading to the formation of the acyl glucuronide metabolite M22. ATZ, a UGT1A1 and UGT1A3 inhibitor, was found to inhibit M22 formation in HLM by up to ~77% with an IC_{50} value of ~4.9 μM, similar to that reported in the literature (data not shown). AZT showed a small inhibition effect of tropifexor metabolism by rhUGT1A9 (maximal inhibition of 37%), suggesting that ATZ is a more selective inhibitor of UGT1A1/3 than UGT1A9. Since UGT1A7 was mainly expressed in gastric tissues and not in the liver (Strassburg CP et al., 1999; Harbourt et al., 2012; Ohtsuki et al. 2012), the contribution of UGT1A7 to the hepatic metabolism of LJN452 was not investigated further. These data suggests that UGT1A1 and UGT1A3 likely contribute to the majority of the glucuronidation of tropifexor in HLM.

The relative contribution of UGT1A1 and UGT1A3 to total tropifexor glucuronidation in HLM was further assessed by determining the kinetics of individual rhUGT metabolism of tropifexor (formation of M22) and scaling the rhUGT $CL_{int,u}$ to HLM $CL_{int,u}$ using a relative expression factor (REF), defined as the ratio of the individual UGT abundance in the rhUGT microsomes relative to its expression in HLM. The $CL_{int,u}$ of individual UGT enzymes was calculated as the quotient of the $V_{max,eff}/K_{m,u}$ obtained from the calculation based on the amount of UGT protein in the incubations (Table 7). The calculated REF values are shown in Table 8. The rhUGT $CL_{int,u}$ of tropifexor from incubations with individual UGT enzymes were then scaled to HLM $CL_{int,u}$. The contribution of individual

DMD Fast Forward. Published on May 5, 2021 as DOI: 10.1124/dmd.120.000349
This article has not been copyedited and formatted. The final version may differ from this version.

UGT enzymes to the overall HLM clearance (percentage of total glucuronidation activity) was then calculated. For the glucuronidation clearance of tropifexor, approximately 84% was estimated to be attributable to UGT1A1 and 16% to UGT1A3 (Table 8).

Estimation of fractional metabolism by CYP and UGT in HH and concentration dependency

Two studies were conducted to assess the relative contributions of CYP and UGT enzymes in HH: chemical inhibition of total CYP or UGT CL_{int} and measurement of individual tropifexor metabolites with time. In both cases, a range of tropifexor concentrations were evaluated. In the first study, the relative contribution of CYP or UGT to the total tropifexor metabolism in the human liver was estimated based on the ability of ABT (a broad non-specific CYP inhibitor), or borneol (with or without ATZ; UGT inhibitors) to inhibit the total metabolism of tropifexor in HH. Tropifexor intrinsic clearance values from HH in the presence of CYP and UGT inhibitors were compared with the sum of intrinsic clearance values. The CL_{int} of tropifexor, at 0.1 µM, in the presence of ABT or a mixture of (+)borneol and ATZ was calculated to be 0.148 or 0.0126 mL/h/million cells, respectively (Table 9). By applying the calculation and normalization methods as described earlier in the method section, the relative contributions of the CYP and UGT enzymes to the total tropifexor metabolism were estimated to be 8% and 92%, respectively (Table 9). The data showed that tropifexor hepatic metabolic pathway is mainly through UGT in vitro at 0.1 µM of tropifexor concentration. However, at a concentration of 0.005 µM, the CL_{int} of tropifexor in the presence of ABT or (-)borneol was calculated to be 0.0337 or 0.0658 mL/h/million cells,

DMD Fast Forward. Published on May 5, 2021 as DOI: 10.1124/dmd.120.000349
This article has not been copyedited and formatted. The final version may differ from this version.

respectively (Table 9) with the relative contributions of CYP and UGT enzymes to the total tropifexor metabolism estimated at approximately 66% and 34%, respectively.

Based upon in vitro metabolic profiles of tropifexor in HH, the contribution of glucuronidation versus oxidative metabolism appeared to vary quantitatively depending on the tropifexor concentration tested (Figure 7; Supplementary Appendix, Table SA04). M22 was the predominant metabolite (~20-30% of the total radioactivity at 4 hours) observed at higher incubation concentrations. As the concentration decreased, the relative abundance of M22 reduced substantially with a concurrent increase in the amounts of the *O*-dealkylation products. At a concentration of 0.1 µM, the amount of M22 (~7.7% of total radioactivity) was similar to that of the *O*-dealkylation products, M10.8 and M11.6 (~7.5% of total radioactivity). At the lowest concentration tested (0.05 µM), the sum of all metabolites containing oxidative transformations (M6.7, M10.8, M11.6 and M18) accounted for ~10.9% of radioactivity, exceeding the amount of M22 observed (~7%).

Discussion and conclusions

The current study was conducted to understand the overall disposition of tropifexor in healthy subjects. Additional in vitro experiments were performed to assess the relative contributions of the possible clearance mechanisms involved and to further evaluate the effects of drug concentration on tropifexor metabolism.

A moderate rate of absorption was achieved (with Cmax 33.5 ng/mL, Tmax 4 hours) following a single oral dose of 1 mg tropifexor. The elimination half-life (13.5 hours) and the overall extent of exposure (AUC_{inf} of 553 h*ng/mL) were in general agreement with

the observations from previous clinical studies (Badman et al., 2020) at a similar dose level.

Mass balance was achieved in all four subjects as demonstrated by the mean total recovery of ~94% (Figure 3), indicating no retention of drug-related residue in humans. No intact tropifexor was observed in the urine from any of the subjects, indicating minimal contribution of renal clearance in tropifexor elimination. This is consistent with the findings in non-clinical species, where no renal clearance of the intact tropifexor was observed. Tropifexor was predominantly eliminated via metabolism in humans, and metabolites of tropifexor were excreted in both feces and urine, with urinary excretion playing a minor role (~28.5% in urine versus ~40% in feces).

Tropifexor was the most prominent drug-related component in plasma, accounting for ~92% of the total radioactivity $AUC_{0\text{-}72h}$. Only minor metabolites, including *O*-dealkylation metabolite M11.6 and the mono-oxidation metabolite M22.4, were found in circulation, contributing to 2-5% of the total radioactivity $AUC_{0\text{-}72h}$. The evaluation of metabolite exposures in human has important implications in drug development. The Food and Drug Administration (FDA), USA guidance on safety testing of drug metabolites (Safety Testing of Drug Metabolites, FDA, April 2020) defined the metabolites requiring further safety testing are those which form at greater than 10% of the total drug-related exposure at steady state. None of the circulating metabolites of tropifexor observed in our study met this criterion; thus, no further safety testing of nonclinical species is warranted. In addition, M11.6 was observed in rat plasma circulating at ~38% of the total radioactivity AUC.

DMD Fast Forward. Published on May 5, 2021 as DOI: 10.1124/dmd.120.000349
This article has not been copyedited and formatted. The final version may differ from this version.

M22.4, although not detected as a circulating metabolite in rats, was observed in dog feces (Supplementary Appendix, Tables SA05 and SA06).

The major biotransformation processes involved in tropifexor metabolism in human appeared to be phase I oxidation, exemplified by metabolites containing at least one oxidative modification accounting for >68% of the radioactivity dose in human excreta. The direct glucuronidation metabolite, M22, was not observed at a quantifiable level in human AME study. Although an acyl-glucuronide is prone to degradation back to the parent under alkaline conditions, a preliminary assessment of M22 stability in human plasma found M22 to be stable, with <5% hydrolyzed back to the parent by 5 hours during an incubation (Supplementary Appendix, Table SA09). Furthermore, no additional mass spectral peak corresponding to M22 molecular ion was observed during the course of incubation, suggesting the absence or low rate of intramolecular acyl-migration under the incubation conditions (Supplementary appendix, Figure SA05). To stabilize acyl-glucuronide in sample matrices, a portion of the human plasma and urine samples were also acidified with formic acid to pH ~4 and processed and analyzed. No quantifiable M22 was observed in these acidified samples. The lack of M22 in human in vivo study was likely not due to metabolite instability in the sample matrices.

Initial in vitro investigations in HLM and HH indicated that glucuronidation was the main contributor to tropifexor metabolism, particularly at the higher tested concentrations of tropifexor. Based on these in vitro results prior to conducting the human AME study, efforts had been focused on identifying the major UGT isozymes responsible for M22 formation and on the drug-drug interaction (DDI) potential of tropifexor with UGT

inhibitors. Consequently, UGT1A1 and UGT1A3 had been identified as the major contributors to tropifexor glucuronidation.

The lack of any quantifiable direct acyl glucuronide metabolites in human in vivo experiments is not surprising given that the acyl glucuronides were likely eliminated via biliary excretion into the gut and subsequently hydrolyzed to the parent tropifexor by microflora. Evidence of biliary elimination of the glucuronide, M22, was apparent from rat ADME studies conducted in intact and bile duct-cannulated (BDC) animals, where M22 was the major metabolite identified in the bile in BDC animals but was absent in intact animals (see Supplementary Appendix; Table SA07 and Table SA08). The labile nature of glucuronide metabolites is not only well documented in the literature (Pellock and Redinbo, 2017), but was also confirmed during an ex vivo assessment in rat and human feces, in which M22 was found to convert back to tropifexor almost completely after 20 hours of incubation under anaerobic conditions (Supplementary Appendix, Table SA010). It is conceivable that M22 could have been formed in the liver, excreted in the bile and passed back into the intestinal tract, where it was de-conjugated by β-glucuronidase expressed in microflora to tropifexor, and was then finally observed as intact tropifexor in feces. It has also been reported that the clearance of a compound in humans via oxidative pathways can be over-estimated in the absence of bile collection when the compound undergoes direct glucuronidation, and where the glucuronides are mainly eliminated via biliary excretion (Wang et al., 2006). In the case of tropifexor, the contribution of oxidative metabolism to the overall tropifexor clearance could have been overestimated in this study due to a lack of information of metabolite in the bile.

DMD Fast Forward. Published on May 5, 2021 as DOI: 10.1124/dmd.120.000349
This article has not been copyedited and formatted. The final version may differ from this version.

Nonetheless, the dominance of the oxidative metabolites in humans (~68% of the dose) appeared to question the translatability of in vitro and non-clinical data. Due to its high potency, tropifexor was given at low doses (0.01 to 3 mg) in the first-in-human study (Badman et al., 2020), with corresponding exposures in the nanomolar range, which were much lower than the micro-molar concentrations used in the initial in vitro studies. One possible explanation of this discrepancy in the in vitro and in vivo studies could be the concentration difference. Tropifexor metabolism at the concentration, where initial in vitro assessment was conducted, may be qualitatively different than that at lower concentrations. To test the hypothesis, additional in vitro experiments covering a wide range of concentrations (0.05 to 10 μM) were conducted. The lower end of this concentration range in HH, 0.05 μM, was chosen to approximate the total C_{max} observed in the clinic at 1-3 mg single dose (C_{max} 22.1-54.2 ng/mL or 0.04-0.09 μM), assuming similar levels of protein binding in the in vitro assay as in vivo, and would likely provide a clinically relevant approximation of the relative contributions of the oxidative and glucuronidation pathways. The results in HH showed that the relative contributions of enzymes (oxidation vs. glucuronidation) to tropifexor metabolism indeed appeared to be concentration dependent (Figure 7). At higher incubation concentrations, direct glucuronidation was undoubtedly the predominant pathway involved. However, when tropifexor concentration was reduced to approach therapeutic exposure levels, although the rates of formation of both glucuronide and oxidative metabolites slowed, the rate of oxidation was higher than that of glucuronidation and became the more important process of the two. This switch of the relative dominance of the two pathways was only apparent when tropifexor concentration was reduced to ≤

DMD Fast Forward. Published on May 5, 2021 as DOI: 10.1124/dmd.120.000349
This article has not been copyedited and formatted. The final version may differ from this version.

0.1 μM. This concentration-dependency of tropifexor metabolism was further confirmed during the in vitro assessment of fractional contributions of CYP and UGT to overall tropifexor metabolism where tropifexor CL_{int} was estimated in the presence and absence of broad specificity UGT or CYP inhibitors. The relative contributions of UGT (fm_{UGT}) and CYP (fm_{CYP}) to tropifexor metabolism at 1 μM were estimated to be 92% and 8%, respectively. This was similar to those observed to the previous in vitro studies, but shifted to 34% (fm_{UGT}) and 66% (fm_{CYP}) at 0.05 μM in line with the predominance of oxidative metabolism observed in this human AME study at similar exposure levels. These in vitro data suggest that tropifexor would be more efficiently metabolized via oxidative pathways than by glucuronidation at clinically relevant concentrations, possibly due to the different affinities and capacities of the CYP and UGT enzymes involved in the metabolism of tropifexor at different doses.

By combining in vitro and in vivo data from various investigations, we now have an understanding of the overall tropifexor disposition in humans (Figure 8). Tropifexor was well absorbed with the absorption estimated at ≥ 73% (normalized to 100% recovery). The major circulating component after an oral dose of tropifexor was the un-changed parent. No circulating metabolite was observed at > 10% of the total AUC. Tropifexor was mainly cleared via metabolism. Phase I oxidation was the predominant tropifexor metabolism pathway, with *O*-dealkylation being the main oxidative process. Although direct glucuronidation was not observed in vivo, its contribution to tropifexor metabolism cannot be ruled out; because the glucuronide metabolite was likely to be eliminated via biliary excretion and converted back to tropifexor in the GI tract. The relative contribution of oxidation was estimated to be 60-100%, while that of glucuronidation

was potentially up to 40%. Tropifexor oxidation was catalyzed mainly by CYP3A4 and CYP2C8 (85-95% and 5-15% relative contribution, respectively), and glucuronidation was catalyzed mainly by UGT1A1 (84%) followed by UGT1A3 (16%). Consequently, there is a potential for tropifexor to undergo DDI with co-medications that are inhibitors or inducers of UGT1A1 and CYP3A. The in vitro metabolism of tropifexor appeared to be concentration-dependent with glucuronidation as the predominant pathway at higher concentrations, and the oxidative process becoming more important at lower concentrations near clinical exposure range.

In conclusion, this study demonstrated the importance of carefully designed in vivo and in vitro experiments for better understanding of disposition processes during drug development. The interplay among the different metabolic pathways in the human body can be complex and variable depending on an array of internal and external factors, with concentration being one of the external factors that can be controlled. Therefore, while dealing with compounds of extreme high potency and low doses, as is the case with tropifexor, relevant therapeutic exposure levels must be taken into consideration in the design of in vitro experiments to enable a more accurate assessment reflecting clinically relevant conditions.

Acknowledgements

The authors would like to thank Ms. Alexandra Vargas, Dr. Elina Siirola, and Mr. Fabian Eggimann for assessing the stability of tropifexor and its glucuronide metabolite M22 in feces and their support for the in vitro production of metabolite standards; and Dr. Tapan Ray for his analytical guidance on the chemical synthesis of radio-labeled tropifexor for clinical use. The authors thank Twarita Chakraborty and Aparajita Mandal,

Novartis Healthcare Pvt. Ltd., for medical writing support and editorial assistance. The authors also acknowledge the clinical research unit of Covance for conducting in-life part of the clinical study as well as its DMPK laboratory for radioactivity analysis of clinical samples.

Authorship Contributions

Participated in research design: LW-L, ZM, HG, JG, EM, GM, HJE, JC

Conducted experiments: LW-L, ZM, LW, HG

Contributed new reagents or analytical tools:

Performed data analysis: LW-L, ZM, LW, HG, MK, HJE, GC, JC

Wrote or contributed to the writing of the manuscript: LW-L, HG, MK, JC, MW, RW, HJE, GC, JC

References

Badman MK, Chen J, Desai S, Vaidya S, Neelakantham S, Zhang J, et al. (2020) Safety, tolerability, pharmacokinetics, and pharmacodynamics of the novel non-bile acid FXR agonist tropifexor (LJN452) in healthy volunteers. Clinical Pharmacol Drug Dev.9 (3):395-410.

Calkin AC and Tontonoz P. (2012) Transcriptional integration of metabolism by the nuclear sterolactivated receptors LXR and FXR. Nat Rev Mol Cell Biol. 13(4): 213–224.

Chiang J YL and Ferrell J M. (2018) Bile Acid Metabolism in Liver Pathobiology. Gene Expression. 18(2): 71-87.

Chiang J YL. (2017) Targeting bile acids and lipotoxicity for NASH treatment. Hepatol. Commun. Hepatol. Commun. 1(10): 1002-1004.

Chiang J YL. (2015) Negative Feedback Regulation of Bile Acid Metabolism: Impact on Liver Metabolism and Diseases. Hepatology. 62 (4): 1315-1317.

Harbourt DE, Fallon JK, Ito S, Baba T, Ritter JK, Glish GL, Smith PC (2012) Quantification of human uridine-diphosphate glucuronosyl transferase 1A isoforms in liver, intestine and kidney using nanobore liquid chromatography-tandem mass spectrometry Anal. Chem. 84 (1), 98–105

Hernandez ED, Zheng L, Kim Y, Fang B, Liu B, Valdez RA, et al. (2019) Tropifexor-mediated abrogation of steatohepatitis and fibrosis is associated with the antioxidative gene expression profile in rodents. Hepatol. Commun. 3(8):1085-1097.

Jinno N, Tagashira M, Tsurui K, Yamada S (2014) Contribution of cytochrome P450 and UDT-glucuronosyltransferase to the metabolism of drugs containing carboxylic acid

groups: risk assessment of acylglucuronides using human hepatocytes, Xenobiotica, 44:8, 677-686.

Meadows V, Kennedy L, Kundu, D, Alpini G, Francis F (2020) Bile acid receptor therapeutic effects on Chronic liver diseases. Frontiers in Medicine. 7:15. DOI: 10.3389/fmed.2020.00015

Neuschwander-Tetro BA, Loomba R, Sanyal AJ, Lavine JE, Van Natta ML, Abdelmalek MF, Chalaani N, Dasarathy S. (2015) Farnesoid X nuclear receptor ligand obeticholic acid for non-cirrhotic, non-alcoholic steatohepatitis (FLINT): a multicentre, randomised, placebo-controlled trial. Lancet. 385(9972): 956–965.

Ohtsuki S, et al (2012) Simultaneous Absolute Protein Quantification of Transporters, Cytochromes P450, and UDP-Glucuronosyltransferases as a Novel Approach for the Characterization of Individual Human Liver: Comparison with mRNA Levels and Activities Drug metabolism and Disposition 40: 83-92.

Parks DJ, Blanchard SG, Bledsoe RK, et al. (1999) Bile acids: Natural ligand for an orphan nuclear receptor. Science. 284(5418):1365-1368.

Pellock SJ, Redinbo MR (2017) Glucuronides in the gut: sugar-driven symbioses between microbe and host. J. Biol. Chem.; 292:8569-8576.

Polyzos SA, Kountouras J, Mantzoros CS. (2020) Obeticholic acid for the treatment of nonalcoholic steatohepatitis: Expectations and concerns. Metabol. Clin. Experimtl. 104:154144

Ratziu V, Sanyal AJ, Loomba R, Rinella M, Harrison S, Anstee QM, et al. (2019) REGENERATE: Design of a pivotal, randomised, phase 3 study evaluating the safety

and efficacy of obeticholic acid in patients with fibrosis due to nonalcoholic steatohepatitis. Contemp. Clin. Trials. 84: 105803.

Safety Testing of Drug Metabolites Guidance for Industry. FDA. www.fda.gov. Accessed on Oct 12, 2020.

Schaap FG, Trauner M, Jansen PL. (2014) Bile acid receptors as targets for drug development. Nat. Rev. Gastroenterol. Hepatol. 11: 55–67.

Strassburg CP, Strassburg A, Nguyen N, Li Q, Manss MP, Tukey RH. (1999) Regulation and function of family 1 and family 2 UDPglucuronosyltransferase genes (UGT1A, UGT2B) in human oesophagus. Biochem. J. 338:489-498.

Tully DC, Rucker PV, Chianelli D, Williams J, Vidal A, Alper PB, et al. (2017) Discovery of tropifexor (LJN452), a highly potent non-bile acid FXR agonist for the treatment of cholestatic liver diseases and nonalcoholic steatohepatitis (NASH). J. Med. Chem. 60: 9960-9973.

Walters JRF, Johnston IM, Nolan JD, Vassie C, Pruzanski ME, Shapiro DA (2015) The response of patients with bile acid diarrhoea to the farnesoid X receptor agonist obeticholic acid. Aliment Pharmacol Ther. 41: 54–64

Wang L, Zhang D, Swaminathan A, Xue Y, Cheng PT, Wu S, Mosqueda-Garcia R, et al. (2006) Glucuronidation as a major metabolic clearance pathway of ^{14}C-labeled muraglitazar in humans: metabolic profiles in subjects with or without bile collection. Drug Metab Dispos 34: 427-439.

Younossi ZM, Ratziu V, Loomba R, Rinella M, Anstee QM, Goodman Z, et al (2019) Obeticholic acid for the treatment of non-alcoholic steatohepatitis: interim analysis from a multicentre, randomised, placebo-controlled phase 3 trial. Lancet. 394: 2184-96.

Zhang D, Chando TJ, Everett DW, Patten CJ, Dehal SS, and Humphreys WG (2005) In vitro inhibition of UDP glucuronosyltransferases by atazanavir and other HIV protease inhibitors and the relationship of this property to in vivo bilirubin glucuronidation. Drug Metab Dispos 33: 1729–1739

Zhu Y, Liu H, Zhang M, Guo GL. (2016) Fatty liver diseases, bile acids, and FXR. Acta Pharmaceutica Sinica B. 6(5): 409-412.

Footnotes

Novartis Institute of Biomedical Research funded this work.

Financial disclosure statement

All the authors, except ZM and LW, are employees of Novartis. ZM and LW were employed by Novartis during the time when the study was conducted.

DMD Fast Forward. Published on May 5, 2021 as DOI: 10.1124/dmd.120.000349
This article has not been copyedited and formatted. The final version may differ from this version.

Legends for Figures

Fig. 1. Chemical structure of [^{14}C]tropifexor. Chemical formula (unlabeled) $C_{29}H_{25}F_4N_3O_5S$; Specific activity: 60 µCi/mg (2.22 MBq/mg)

Fig. 2. Arithmetic mean (±SD) of the plasma tropifexor and plasma total radioactivity concentration-time profiles

Fig. 3. Mean (±SD) cumulative excretion of radioactivity in urine and feces following a single oral dose of 1 mg [^{14}C]tropifexor in healthy male subjects (N = 4)

Fig. 4. Representative Tropifexor metabolite profiles in pooled plasma following a single oral dose of 1 mg [^{14}C]tropifexor in healthy subjects

Fig. 5. Representative metabolite profile in urine and feces following a single oral dose of 1 mg [^{14}C] tropifexor in healthy subjects

Fig. 6. Proposed biotransformation pathways of tropifexor

Fig. 7. Rate of [^{14}C]tropifexor glucuronidation and the oxidative pathway over concentration range

Fig. 8. Disposition of tropifexor in humans

DMD Fast Forward. Published on May 5, 2021 as DOI: 10.1124/dmd.120.000349
This article has not been copyedited and formatted. The final version may differ from this version.

Tables

Table 1. Summary statistics of total radioactivity and tropifexor PK parameters in plasma

	Plasma tropifexor	**Plasma total radioactivity**
PK parameter (Unit)	**N=4**	**N=4**
AUC_{inf} (h*ng/mL)[†](h*ng-eq/mL)[‡]	553±110 (19.9%)	674±122 (18.1%)
AUC_{last} (h*ng/mL)[†](h*ng-eq/mL)[‡]	552±110 (20.0%)	652±124 (19.1%)
C_{max} (ng/mL)[†](ng-eq/mL)[‡]	33.5±5.74 (17.2%)	37.9±7.24 (19.1%)
$T_{1/2}$ (h)	13.5±2.04 (15.1%)	20.4±4.49 (22.0%)
T_{max} (h)	4.00 (3.00-4.00)	4.00 (4.00-4.00)
CL/F (mL/h)	1870±439 (23.5%)	
Vz/F (mL)	36400±10300 (28.3%)	

Statistics are Arithmetic Mean ± SD (CV%); CV% = Coefficient of variation (%) = SD/Mean*100; For T_{max}, Statistics are Median (Min-Max)TRA = total radioactivity; [†]Plasma tropifexor; [‡] Plasma total radioactivity.

DMD Fast Forward. Published on May 5, 2021 as DOI: 10.1124/dmd.120.000349
This article has not been copyedited and formatted. The final version may differ from this version.

Table 2. Plasma concentrations and PK parameters of tropifexor and its metabolites following a single oral dose of 1 mg [^{14}C]tropifexor to healthy subjects

Time (h)	M11.6[1]	M22.4[1]	Tropifexor[1]
1	0.0773	--[2]	1.74
2	0.371	0.240	13.1
4	0.832	1.09	35.1
6	0.483	1.01	27.5
8	0.363	1.37	26.7
12	0.308	1.18	19.0
24	--	0.412	7.45
48	0.150	0.249	2.17
72	--	--	0.987
C_{max} (ng-eq/mL)	0.832	1.37	35.1
T_{max} (h)	4	8	4
$AUC_{0\text{-}72h}$[3] (h*ng-eq/mL)	10.4	31.5	576
AUC_{inf} (h*ng-eq/mL)	NC[4]	NC	597
%Total radioactivity $AUC_{0\text{-}72h}$[5]	1.65	5.00	91.6
%Parent $AUC_{0\text{-}72h}$	1.81	5.46	100

[1]The plasma radioactivity concentrations are expressed in ng-eq/mL

[2]Not detected

[3]Calculated using linear trapezoidal method. The concentrations at time zero was taken as zero.

[4]Not calculated

[5]The %total radioactivity AUC for each metabolite is calculated based on the total plasma radioactivity $AUC_{0\text{-}72h}$ of 629 h*ng-eq/mL.

DMD Fast Forward. Published on May 5, 2021 as DOI: 10.1124/dmd.120.000349
This article has not been copyedited and formatted. The final version may differ from this version.

Table 3. The total mean (±SD) recovery of tropifexor and its metabolites in human excreta (expressed as a percentage of the dose) following an oral dose of 1 mg [^{14}C]tropifexor to healthy subjects (N = 4)

	Urine	**Feces**	
Metabolite	**Mean(SD)**	**Mean(SD)**	**Total**
M6	3.23 (1.19)	8.61 (2.81)	11.8
M6.7	1.71 (0.53)	--[1]	1.71
M8.8	10.8 (1.30)	--	10.8
M10.8	3.66 (0.40)	3.34 (0.34)	7.00
M11.6	4.90 (0.82)	6.54 (0.85)	11.4
M18.2	--	2.22 (0.34)	2.22
M18.1	--	2.93 (1.52)	2.93
M22.4+M19.5[2]	--	7.97 (1.65)	7.97
M24	--	2.58 (0.28)	2.58
Tropifexor	--	25.4 (4.67)	25.4
Other[3]	4.17 (1.37)	5.70 (0.24)	9.87
Total	28.5 (2.82)	65.3 (4.13)	93.8

[1] --=Not detected

[2] M22.4 co-eluted with M19.5 in feces. The sum of both components is reported

[3] Sum of small uncharacterized components, each contributing to < 2% of the total dose

DMD Fast Forward. Published on May 5, 2021 as DOI: 10.1124/dmd.120.000349
This article has not been copyedited and formatted. The final version may differ from this version.

Table 4. Mass spectral analysis of tropifexor and its metabolites in human plasma, urine, and feces

Component	Bio-transformation	Theoretical mass[a] *m/z* $[MH]^+$	Matrix	Proposed structure and MS/MS fragments[c]	Characteristics fragments ions
Tropifexor	Parent	606.1556	Pl, Fc	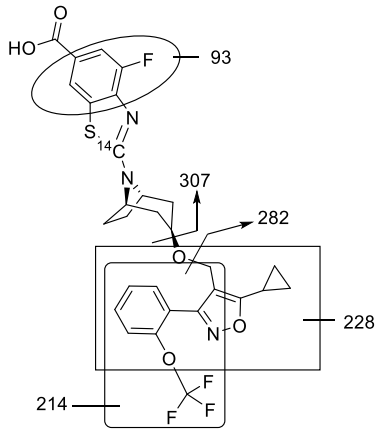	307, 282, 228, 214, and 93
M6	*O*-dealkylation + oxidation	341.0842	Ur, Fc	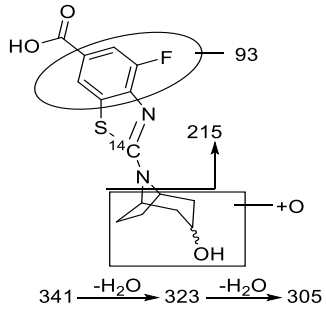	323 (-H_2O), 305 (-$2H_2O$), 215, and 93
M6.7	*O*-dealkylation + glucuronidation	501.1214	Ur	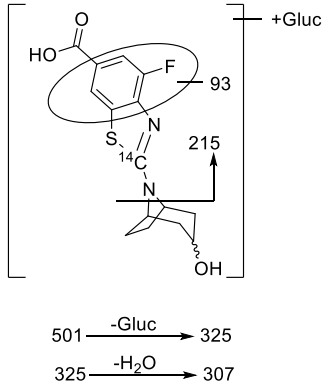	325 (-$C_6H_8O_6$), 307 (-$C_6H_8O_6$, -H_2O), 215, and 93

DMD Fast Forward. Published on May 5, 2021 as DOI: 10.1124/dmd.120.000349
This article has not been copyedited and formatted. The final version may differ from this version.

M8.8	*O*-dealkylation + glucuronidation	501.1214	Ur	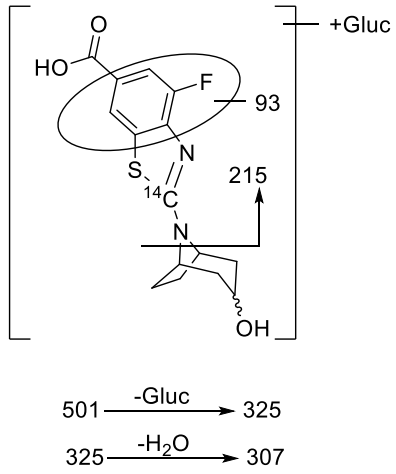	325 (-C_6H_8O) 307 (-$C_6H_8O_6$, -H_2O), 215, and 93
M10.8	*O*-dealkylation	325.0893	Ur, Fc	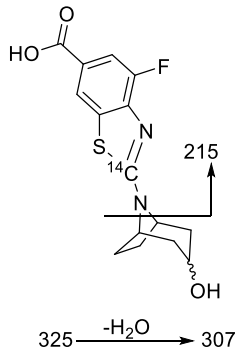	307 (-H_2O) and 215
M11.6	*O*-dealkylation	325.0893	Pl, Ur, Fc	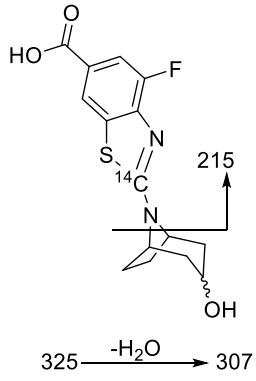	307 (-H_2O) and 215

M18.2	Di-oxidation	638.1455	Fc	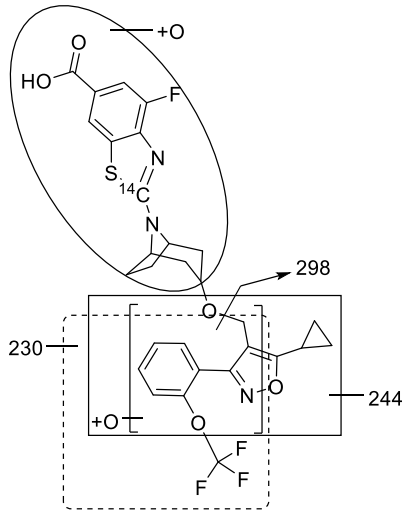	298, 244, and 230
M18.1	Di-oxidation + Hydrogenation	640.1611	Fc	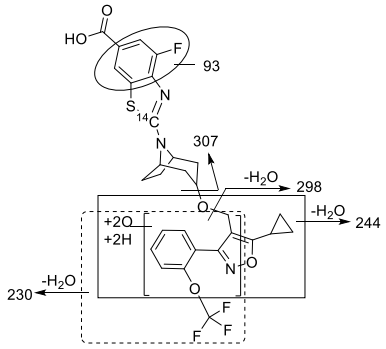	307, 230, 244, 298, and 93
M22	Glucuronidation	782.1877	PI (trace[b])	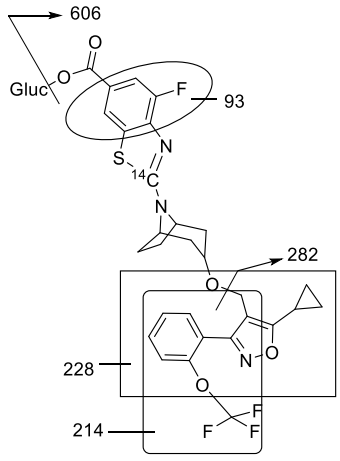	606 (-$C_6H_8O_6$), 282, 228, 214, and 93

DMD Fast Forward. Published on May 5, 2021 as DOI: 10.1124/dmd.120.000349
This article has not been copyedited and formatted. The final version may differ from this version.

M22.4	Oxidation	622.1505	Pl, Fc	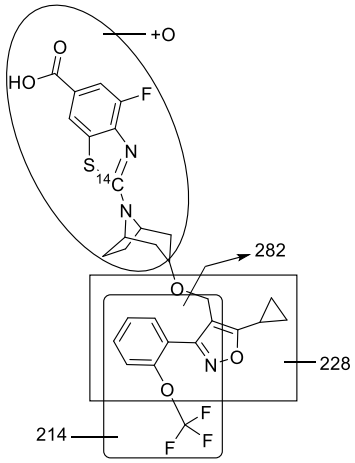	282, 228, and 214
M19.5	Di-oxidation	638.1455	Fc	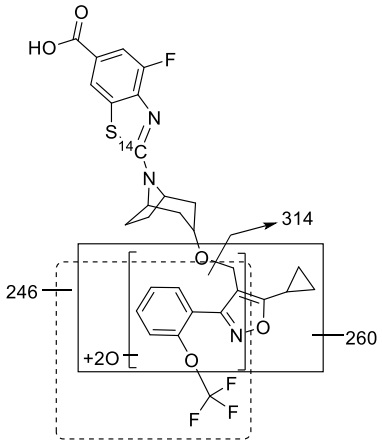	314, 260, and 246
M24	Oxidation	622.1505	Fc	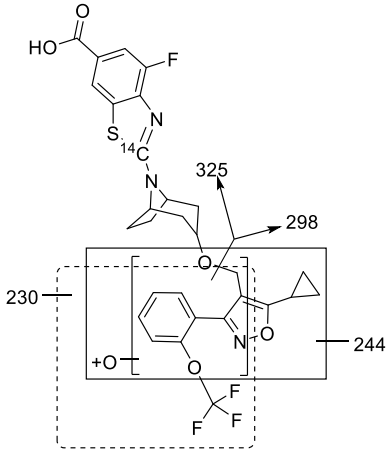	298, 244, and 230

DMD Fast Forward. Published on May 5, 2021 as DOI: 10.1124/dmd.120.000349
This article has not been copyedited and formatted. The final version may differ from this version.

Table 5. Relative contributions of CYP enzymes to tropifexor oxidative metabolism in HLM using CYP-selective chemical inhibition

Enzyme	Inhibition	CL_{int} (mL/h/mg protein)	Experimental *fm* (%)	Corrected fm_{CYP} (%)[a]	Normalized fm_{CYP} (%)[b]
	No inhibition	0.223			
CYP2C8	Montelukast (2 µM)	0.145	34.9	12.8	15
CYP2C9	Sulfaphenazole (5 µM)	0.209	6.07	-1.16	0[c]
CYP3A	Ketoconazole (1 µM)	0.0577	74.1	72.6	85

[a]Experimental fm_{CYP} was corrected with inhibitor cross-reactivity as described in the materials and methods. [b]Corrected fm_{CYP} was normalized to a total of 100%. [c]Negative fm_{CYP} value after correction were considered to be analytical artifacts and set as 0.

DMD Fast Forward. Published on May 5, 2021 as DOI: 10.1124/dmd.120.000349
This article has not been copyedited and formatted. The final version may differ from this version.

Table 6. Contributions of CYP enzymes to tropifexor oxidative metabolism in HLM determined by rhCYP kinetics and scaling using a RAF

CYP **(and protein) concentration in incubation** pmol CYP·mL^{-1} (mg microsomal protein·mL^{-1})	**Half-life T½ (**min)	**fu_{mic}**[a]	**$CL_{int,u}$**[b] mL·h^{-1}·mg microsomal protein^{-1}	**$CL_{int,u}$ /RAF**[c] mL·h^{-1}·mg microsomal protein^{-1}	**% Of the total CYP contribution**
CYP2C8 200 (0.620)	15.7	0.0282	151	5.30	5%
CYP3A4 200 (1.82)	5.20	0.0150	293	94.3	95%

[a]fu_{mic} for tropifexor was determined by the equation fu_{mic}=0.0350-0.0110*[protein], where the protein concentration range was 0.5-2 mg/mL (see Supplemental Information); [b]unbound CL_{int} (CL_{int}/fu_{mic}); [c]RAF, relative activity factor. The value was calculated as 28.5 and 3.11 for CYP2C8 and CYP3A4, respectively see Supplemental Table SA02.

DMD Fast Forward. Published on May 5, 2021 as DOI: 10.1124/dmd.120.000349
This article has not been copyedited and formatted. The final version may differ from this version.

Table 7. Kinetic parameters for tropifexor metabolism by rhUGT enzymes

Tropifexor glucuronidation (M22 formation)	**Total K_m** μM (unbound $K_{m,u}$)[a]	**V_{max}** nmol·h^{-1}·mg protein^{-1}	**$V_{max,eff}$**[b] nmol·h^{-1}·mg protein^{-1}
UGT1A1	38.4 ± 14.1 (1.22 ± 0.45)	58.9 ± 16.1	24
UGT1A3	21.4 ± 4.05 (0.68 ± 0.13)	18.6 ± 1.96	12

[a]Values in parentheses are the unbound K_m (K_m value* fu_{mic}); fu_{mic} for tropifexor was determined to be 0.0318 for an incubation of 0.50 mg protein·mL^{-1}

[b]Effective V_{max}, highest mean total [^{14}C]tropifexor metabolism activities detected in the kinetics studies

The unbound K_i = K_i* fu_{mic} = 53.2 and 250 μM for UGT1A1 and UGT1A3, respectively.

DMD Fast Forward. Published on May 5, 2021 as DOI: 10.1124/dmd.120.000349
This article has not been copyedited and formatted. The final version may differ from this version.

Table 8. Contribution of individual UGT enzymes to tropifexor clearance in HLM

UGT	Expression level (nmol UGT/mg microsomal protein)[a]	REF (rhUGT/HLM)	$CL_{int,u}$ ($V_{max,eff}/K_{m,u}$) $mL \cdot h^{-1} \cdot nmol\ UGT^{-1}$	Scaled HLM $CL_{int,u}$/REF ($mL \cdot h^{-1} \cdot mg\ HLM\ protein^{-1}$)	Contribution to HLM CL (%)
rhUGT1A1	0.834	15.4	19.4	1.26	84
UGT1A1 (HLM)	0.054				
rhUGT1A3	0.754	73.2	17.9	0.244	16
UGT1A3 (HLM)	0.0103				

[a]Values are the expression level of rhUGT enzymes from the specific lots used in the rhUGT kinetic study, as well as in HLM (nmol UGT enzyme per mg protein)

DMD Fast Forward. Published on May 5, 2021 as DOI: 10.1124/dmd.120.000349
This article has not been copyedited and formatted. The final version may differ from this version.

Table 9. Estimated fractional metabolism values of the tropifexor metabolism pathways in HH using CYP or UGT inhibitors

Tropifexor concentration	**Pathway**	**Inhibitor**[a] (concentration)	**CL_{int}** (mL/h/million cells)	**Estimated fm** (%)[b]
0.1 μM	CYP	ABT (3.0 mM)	0.148	8
	UGT	(+) Borneol (500 μM) ATZ (50 μM)	0.0126	92
	Total[c]		0.160	100
0.005 μM	CYP	ABT (3.0 mM)	0.0337	66
	UGT	(-) Borneol (500 μM)	0.0658	34
	Total[c]		0.0995	100

[a]ABT inhibits CYPs while borneol inhibits UGTs (Jinno et al 2014) and ATZ inhibits UGT1A1/3 (Zhang et al 2005);

[b]$(CL_{int} - CL_{int,(+\text{ inhibitor})})/CL_{int}$ x100%

[c]Sum of $CL_{int,(+CYP\text{ inhibitor})}$ and $CL_{int,(+UGT\text{ inhibitor})}$

DMD Fast Forward. Published on May 5, 2021 as DOI: 10.1124/dmd.120.000349
This article has not been copyedited and formatted. The final version may differ from this version.

Figure 1

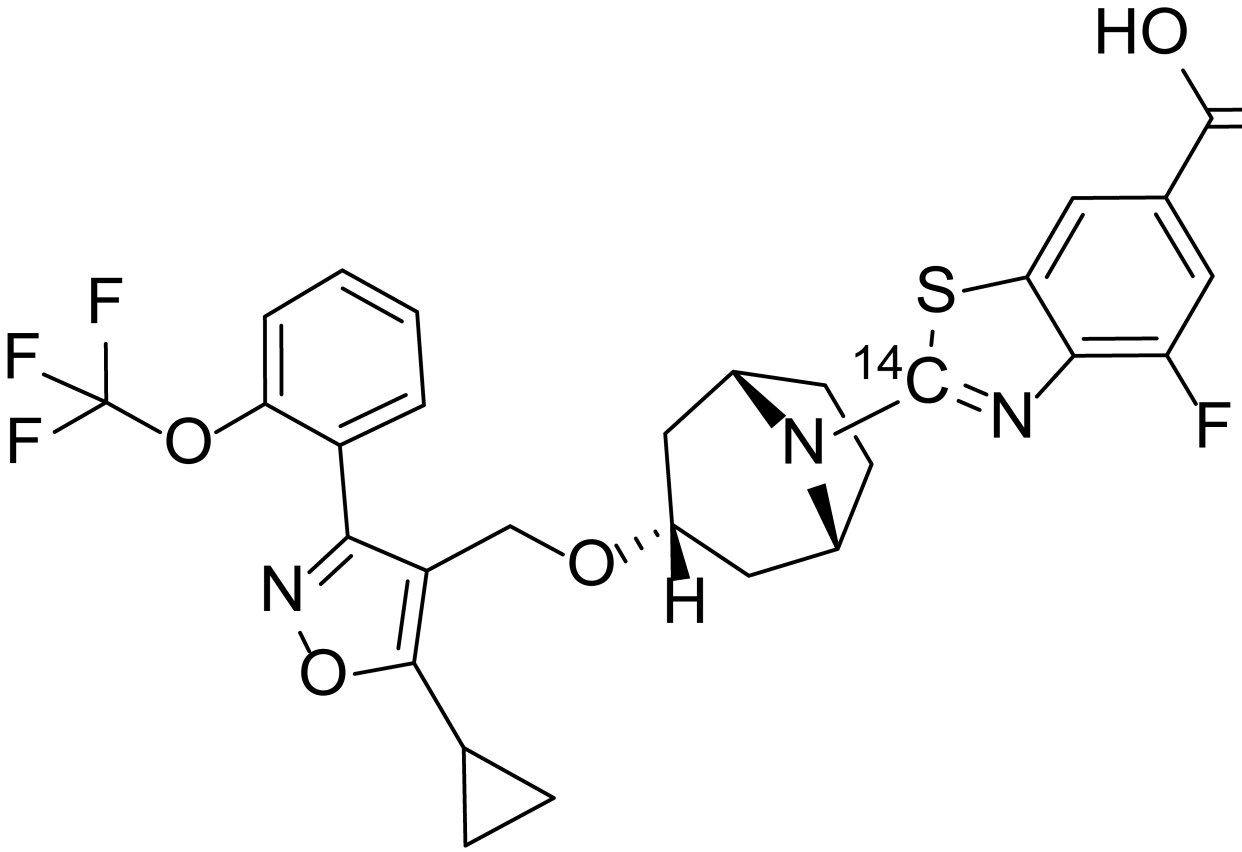

Chemical formula (unlabeled) C29H25F4N3O5S;
Specific activity: 60 μCi/mg (2.22 MBq/mg)

Figure 2.

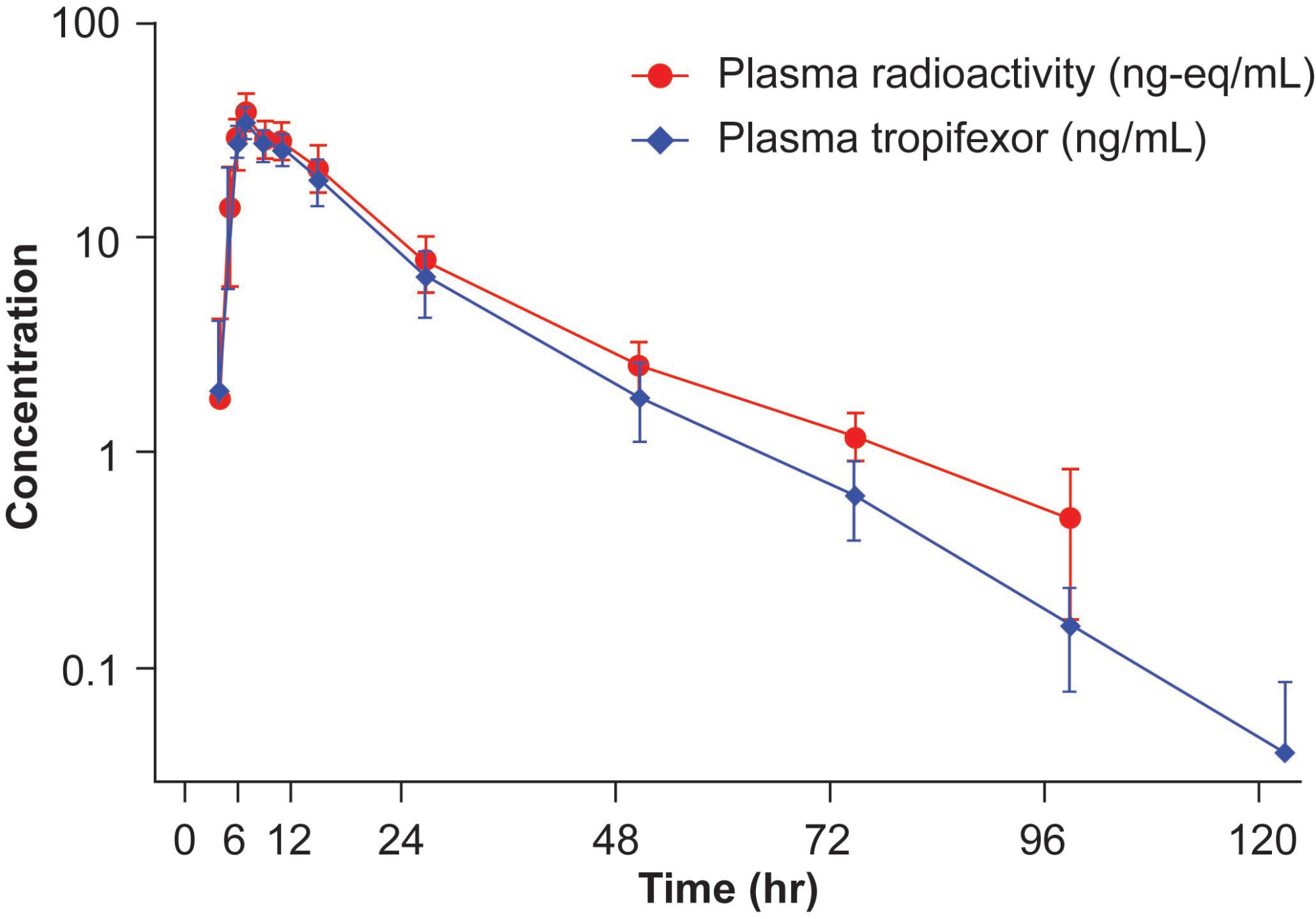
100
10
1
0.1
Concentration
Plasma radioactivity (ng-eq/mL)
Plasma tropifexor (ng/mL)
0
6
12
24
48
72
96
120
Time (hr)

Figure 3.

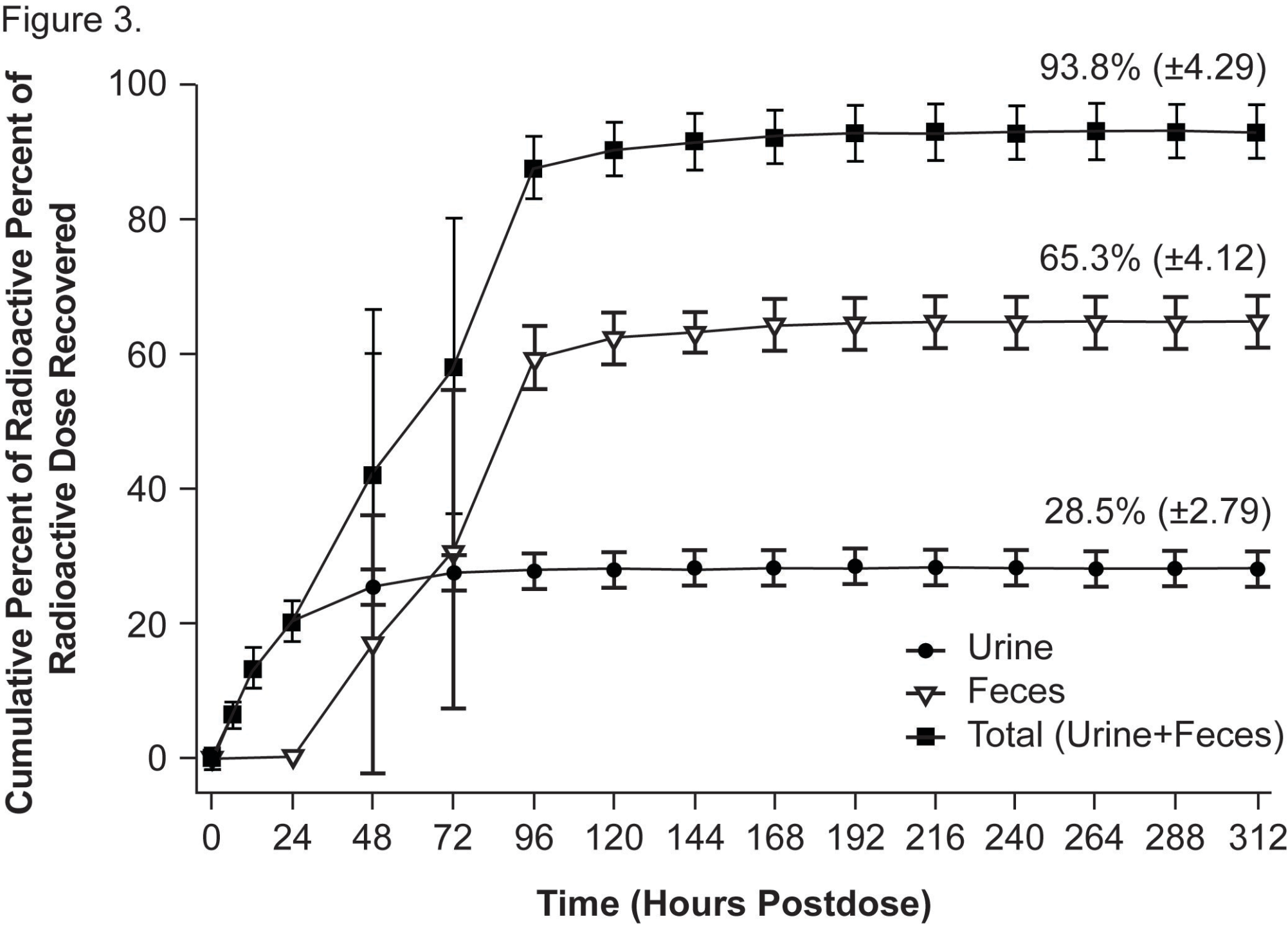
93.8% (±4.29)
65.3% (±4.12)
28.5% (±2.79)
Urine
Feces
Total (Urine+Feces)
Cumulative Percent of Radioactive Dose Recovered
Cumulative Percent of Radioactive Dose Recovered
Time (Hours Postdose)
0
20
40
60
80
100
0
24
48
72
96
120
144
168
192
216
240
264
288
312

Figure 4

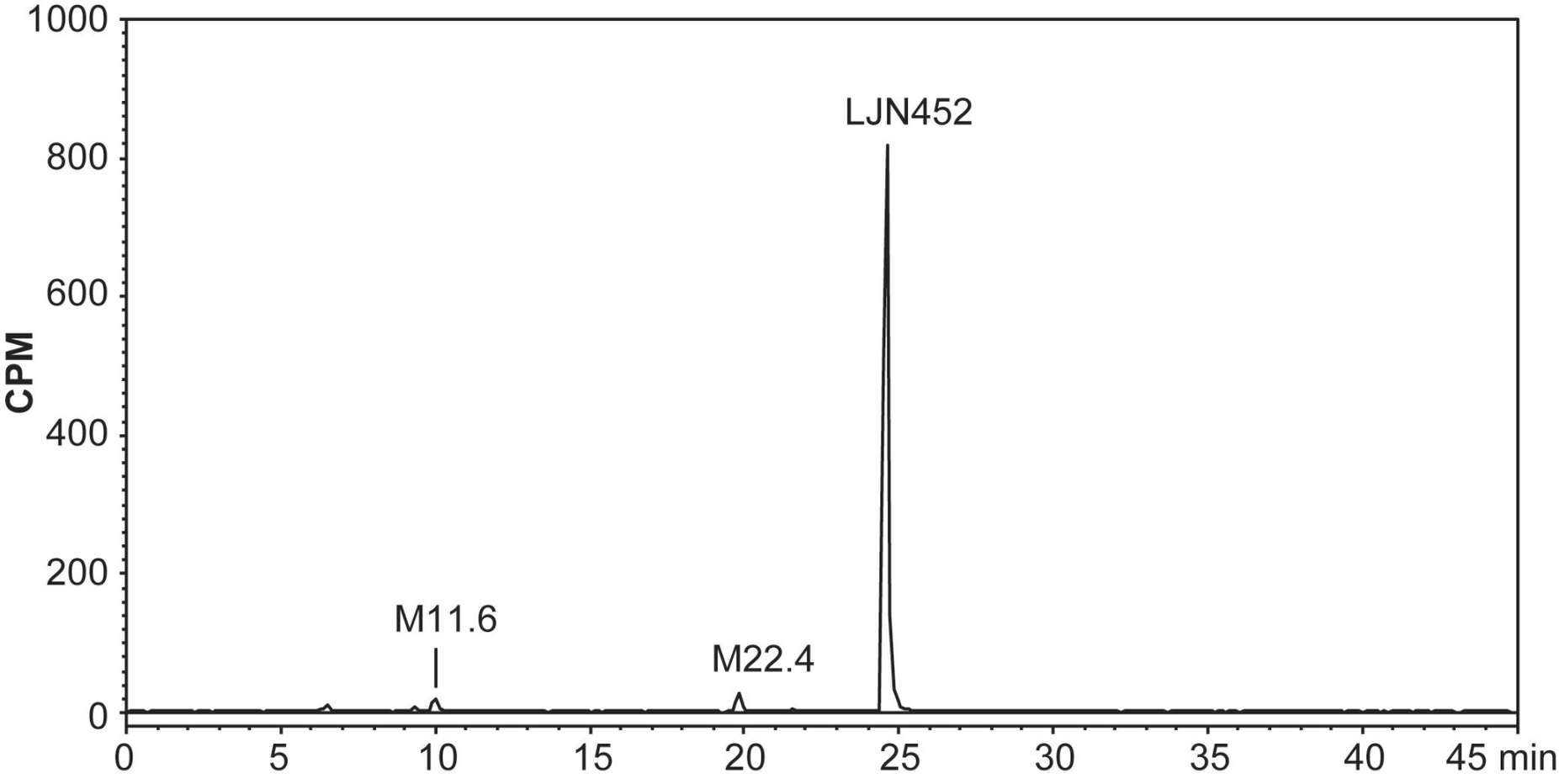
1000
800
600
400
200
0
CPM
LJN452
M11.6
M22.4
0
5
10
15
20
25
30
35
40
45 min

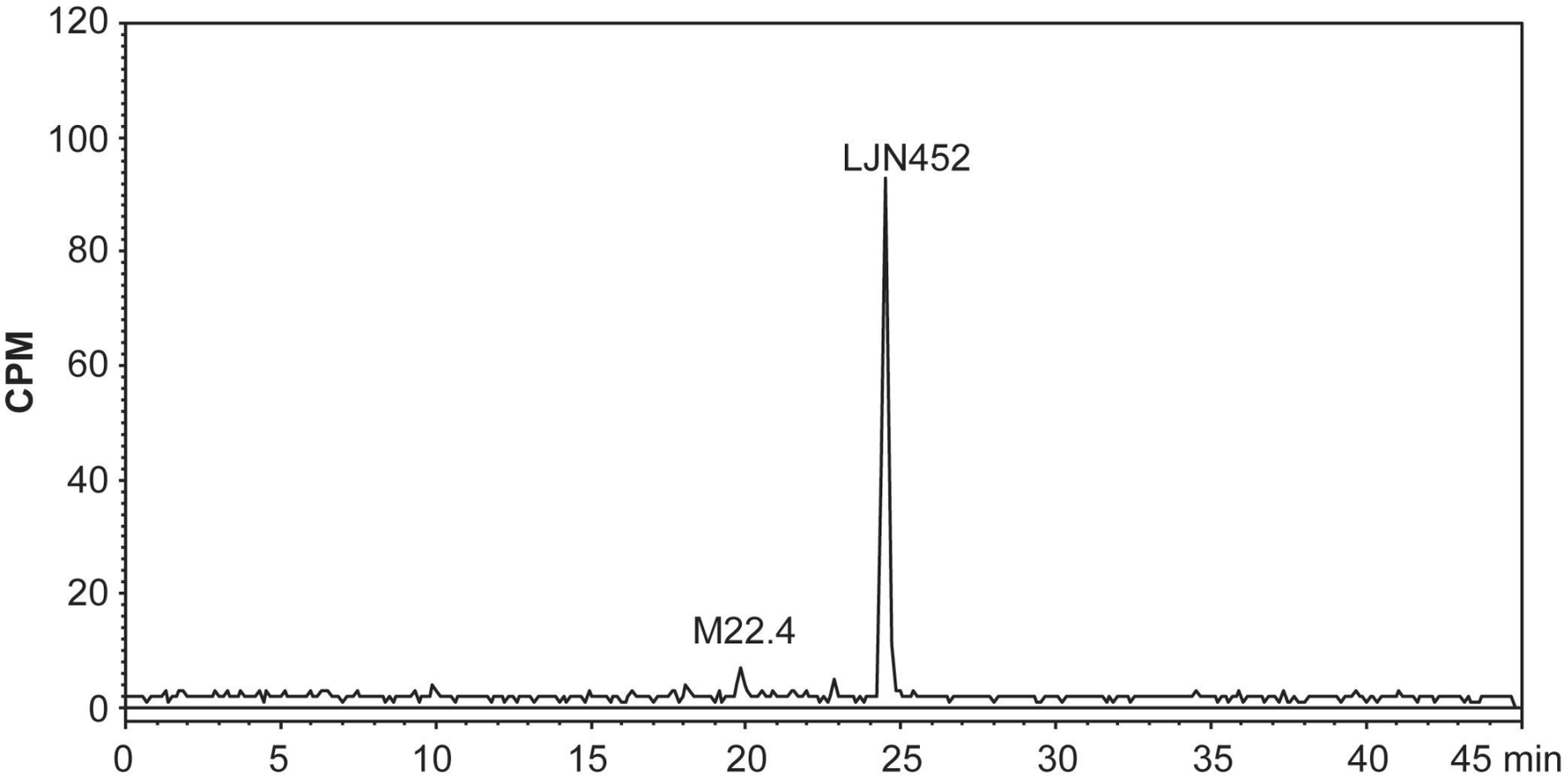
120
100
80
60
40
20
0
CPM
LJN452
M22.4
0
5
10
15
20
25
30
35
40
45 min

Figure 5.

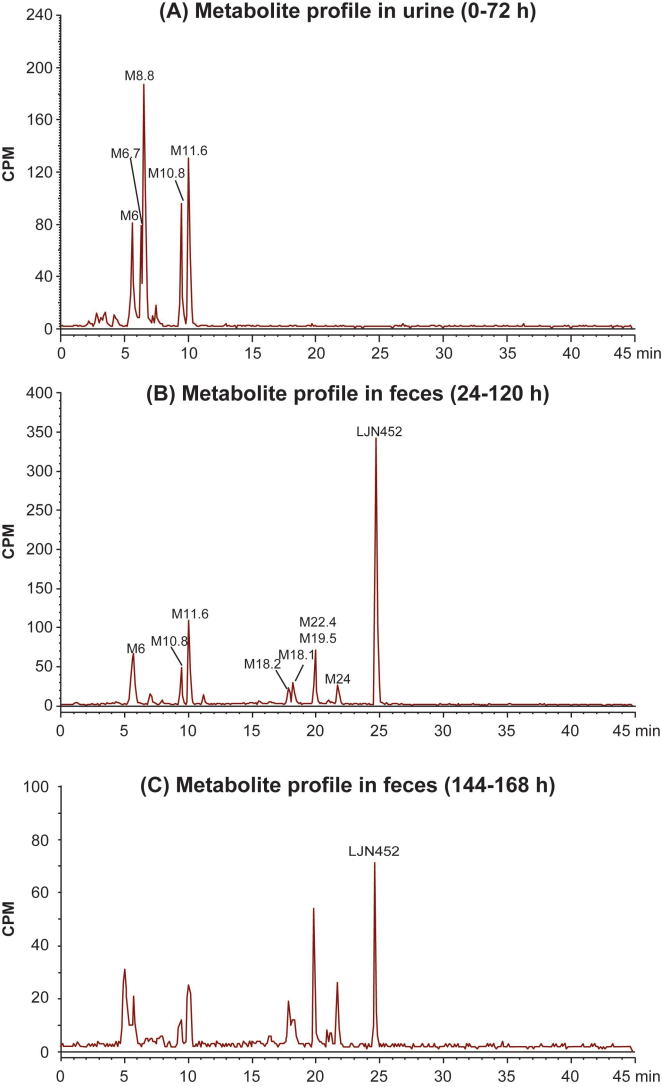
(A) Metabolite profile in urine (0-72 h)
CPM
240
200
160
120
80
40
0
M8.8
M6.7
M11.6
M10.8
M6
0
5
10
15
20
25
30
35
40
45 min
(B) Metabolite profile in feces (24-120 h)
CPM
400
350
300
250
200
150
100
50
0
LJN452
M11.6
M22.4
M19.5
M6
M10.8
M18.2
M18.1
M24
0
5
10
15
20
25
30
35
40
45 min
(C) Metabolite profile in feces (144-168 h)
CPM
100
80
60
40
20
0
LJN452
0
5
10
15
20
25
30
35
40
45 min

Figure 6.

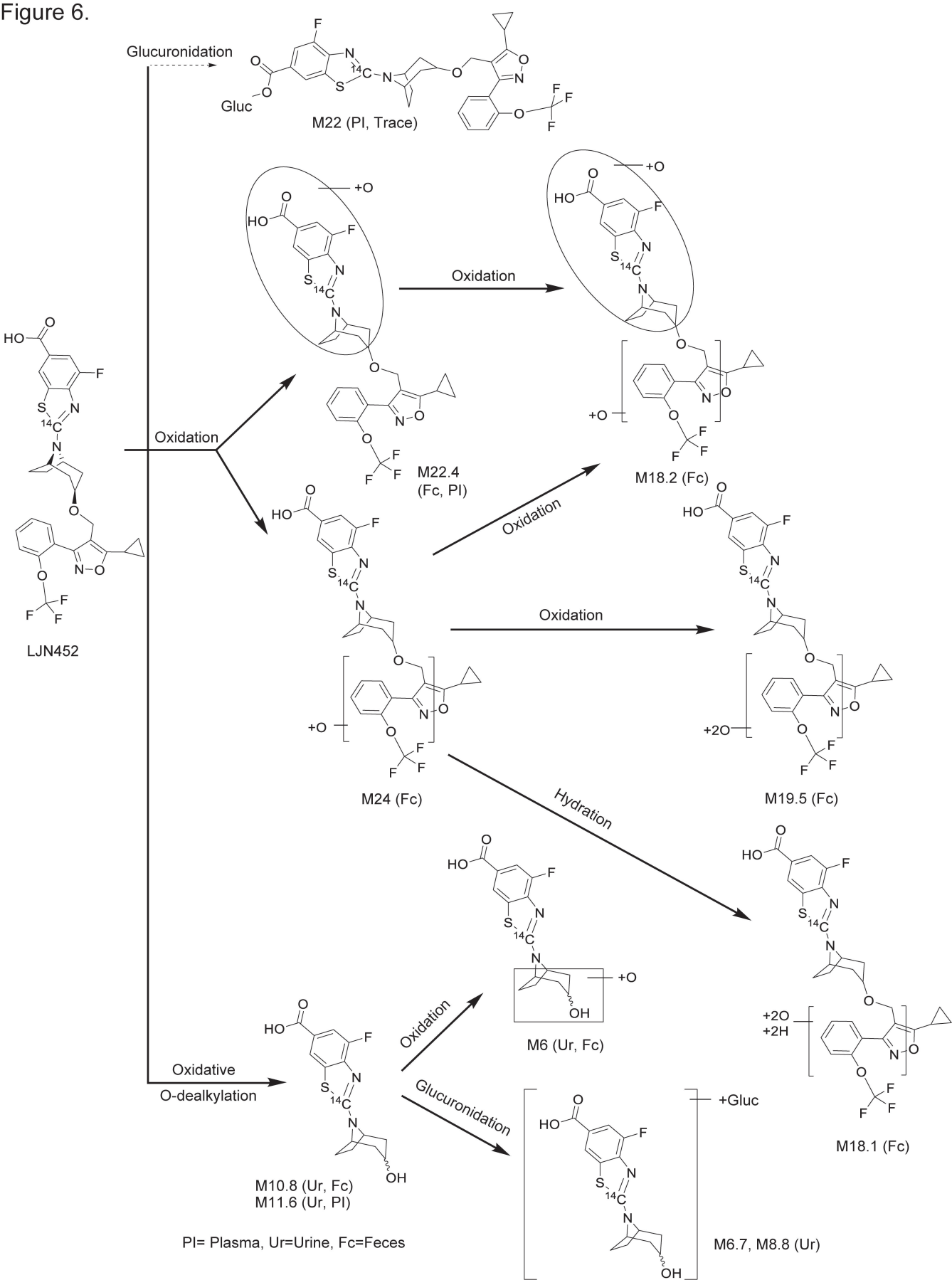
Glucuronidation
Gluc
M22 (PI, Trace)
Oxidation
M22.4
(Fc, PI)
Oxidation
M18.2 (Fc)
LJN452
Oxidation
Oxidation
M24 (Fc)
Oxidation
M19.5 (Fc)
Hydration
M6 (Ur, Fc)
Oxidative
O-dealkylation
Oxidation
Glucuronidation
+Gluc
M18.1 (Fc)
M10.8 (Ur, Fc)
M11.6 (Ur, PI)
M6.7, M8.8 (Ur)
PI= Plasma, Ur=Urine, Fc=Feces

Figure 7.

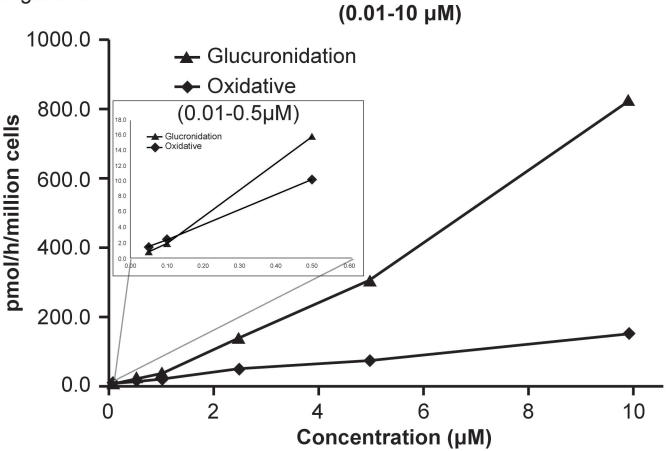

*Concentration (µM)	0.05	0.10	0.50	1.0	2.5	5.0	10.0
Glucuronidation formation rate (pmol/h/million/cells) **(a)**	0.873	1.92	15.9	30.3	134	300	821
†Qxidative pathway formation rate (pmol/h/million/cells) **(b)**	1.4	2.4	10.3	17.5	47.3	68.8	149
Ratio of the formation rate **(a/b)**	0.6	0.8	1.5	1.7	2.8	4.4	5.5

†Nominal concentration: †oxidative pathway includes O-dealkylation (M10.8. M11.6) and secondary metabolites(M6.7. M18)

Figure 8.

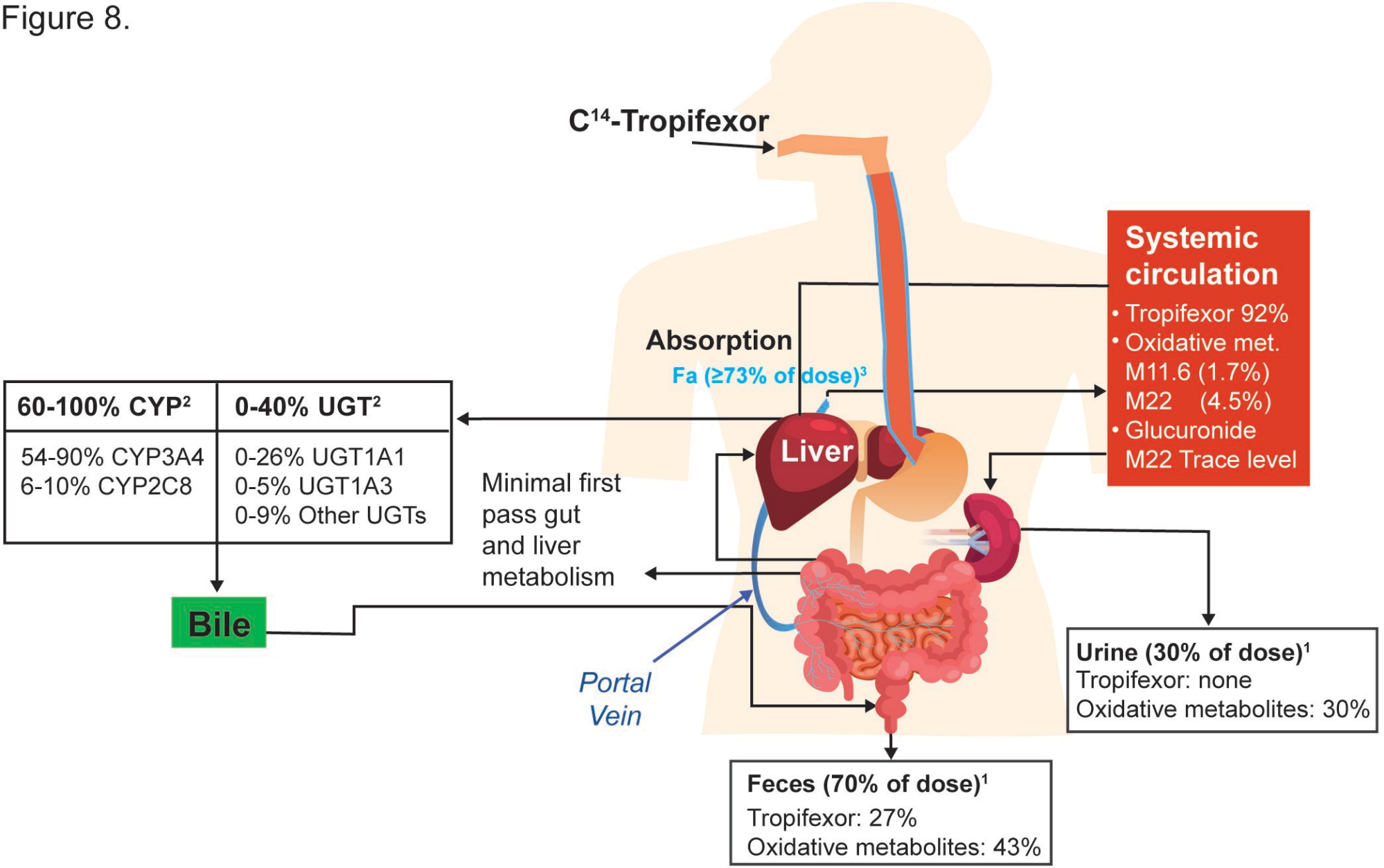

[1]The route of excretion was ~70% in feces and ~30% in urine (normalized to 100%); the range unabsorbed tropifexor was estimated based on the % of parent in feces assuming the parent in feces was absorbed and had been converted from glucuronide.

[2]The relative contribution by CYP and UGT were estimated to be 60-100% and 0-40%, respectively, where the combination of de-alkylation and glucuronidation metabolites in urine were considered as primary oxidative (low end) and glucuronide (high end) metabolites, respectively. Additionally, CYP3A4 and CYP2C8 in HLM was estimated to be 90% and 10%, respectively, and the relative contribution by UGT1A1/UGT1A3 and other UGTs in HLM was estimated to be 77% of and 23%, respectively , and UGT1A1 and UGT1A3 in HLM was estimated to be 84% and 16%, respectively. Together, the relative contribution of UGT1A1, UGT1A3, and other UGTs in HLM was estimated to be 65%, 12%, and 23%, respectively.

[3]The absorption and bioavailability (73-100%) were estimated based on the assumption that 27% tropifexor in feces was unabsorbed (low end) and 27% of tropifexor absorbed and converted from glucuronide metabolite (high end).

DMD Fast Forward. Published on May 5, 2021 as DOI: 10.1124/dmd.120.000349
This article has not been copyedited and formatted. The final version may differ from this version.

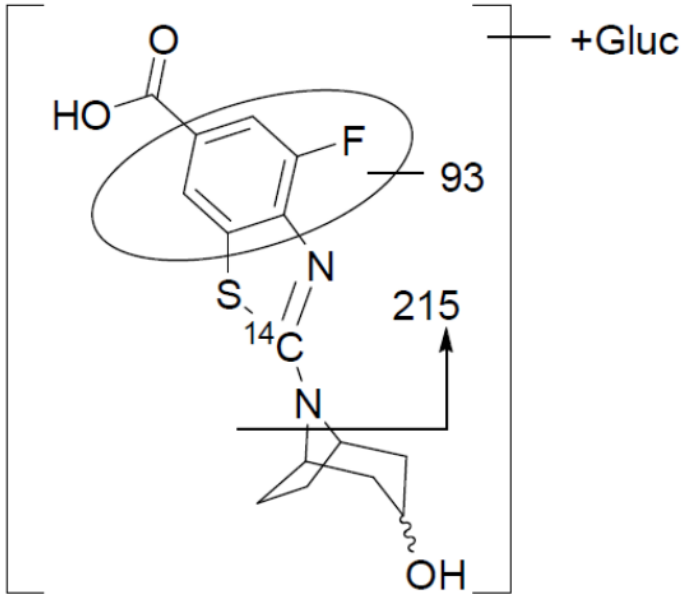

501 —(-Gluc)→ 325

325 —(-H_2O)→ 307

DMD Fast Forward. Published on May 5, 2021 as DOI: 10.1124/dmd.120.000349
This article has not been copyedited and formatted. The final version may differ from this version.

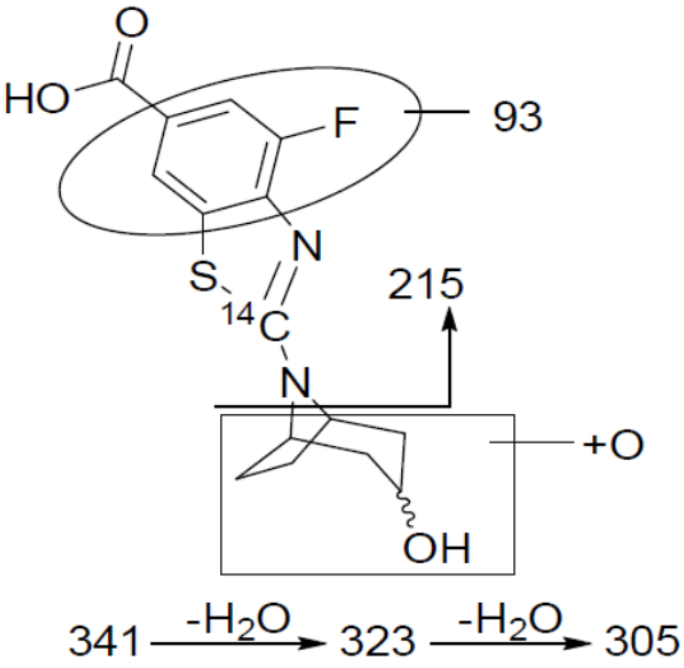

DMD Fast Forward. Published on May 5, 2021 as DOI: 10.1124/dmd.120.000349
This article has not been copyedited and formatted. The final version may differ from this version.

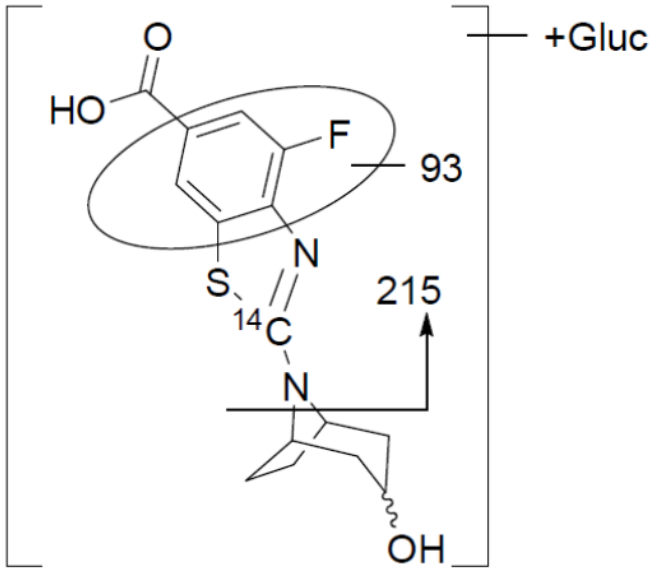

501 -Gluc→ 325

325 -H_2O→ 307

DMD Fast Forward. Published on May 5, 2021 as DOI: 10.1124/dmd.120.000349
This article has not been copyedited and formatted. The final version may differ from this version.

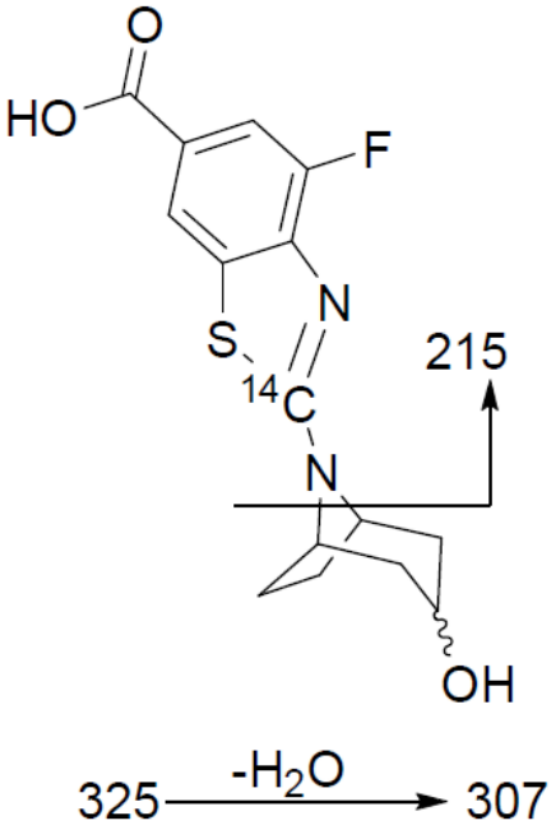

DMD Fast Forward. Published on May 5, 2021 as DOI: 10.1124/dmd.120.000349
This article has not been copyedited and formatted. The final version may differ from this version.

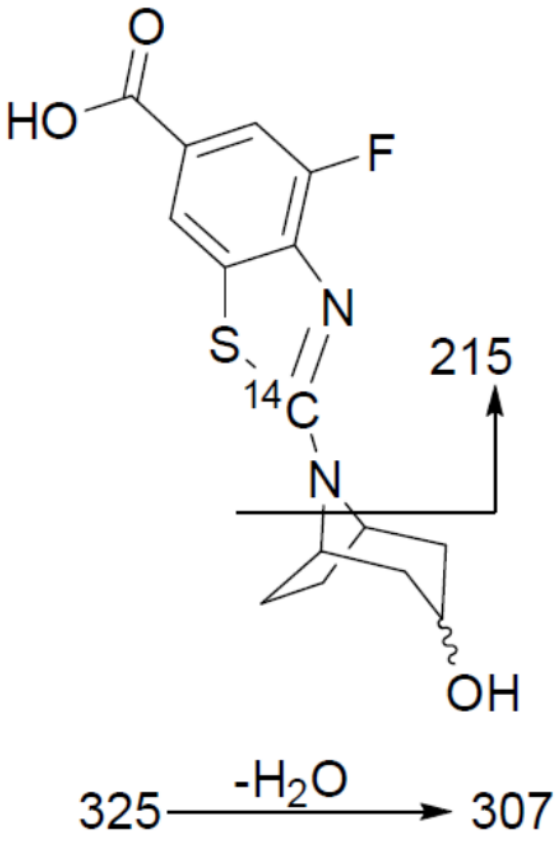

DMD Fast Forward. Published on May 5, 2021 as DOI: 10.1124/dmd.120.000349
This article has not been copyedited and formatted. The final version may differ from this version.

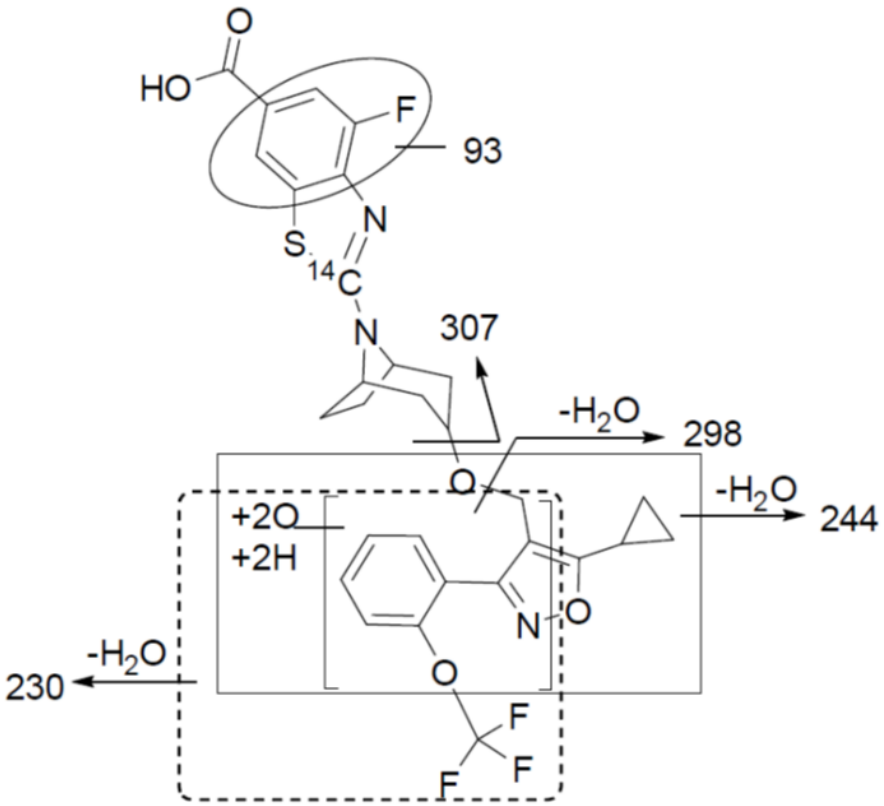

DMD Fast Forward. Published on May 5, 2021 as DOI: 10.1124/dmd.120.000349
This article has not been copyedited and formatted. The final version may differ from this version.

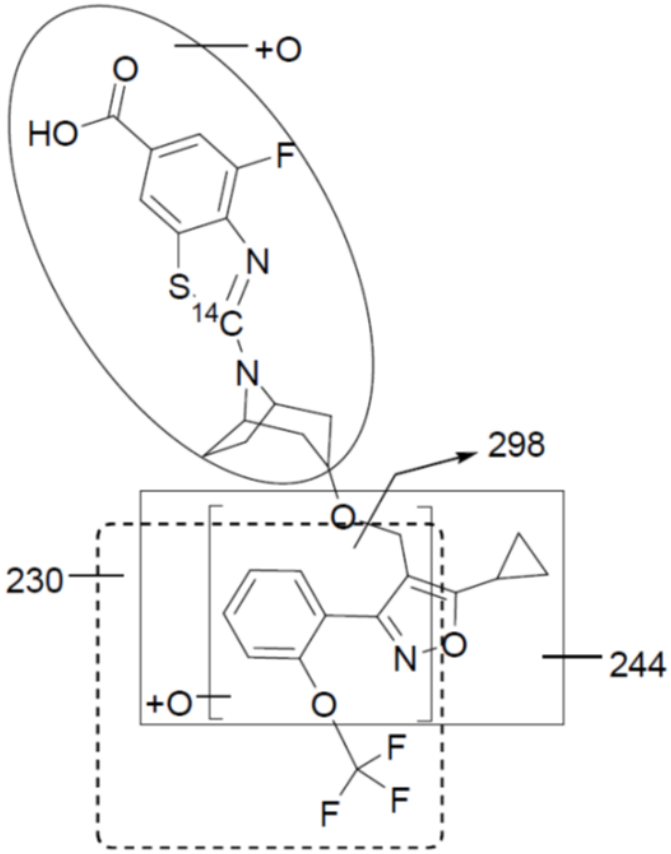

DMD Fast Forward. Published on May 5, 2021 as DOI: 10.1124/dmd.120.000349
This article has not been copyedited and formatted. The final version may differ from this version.

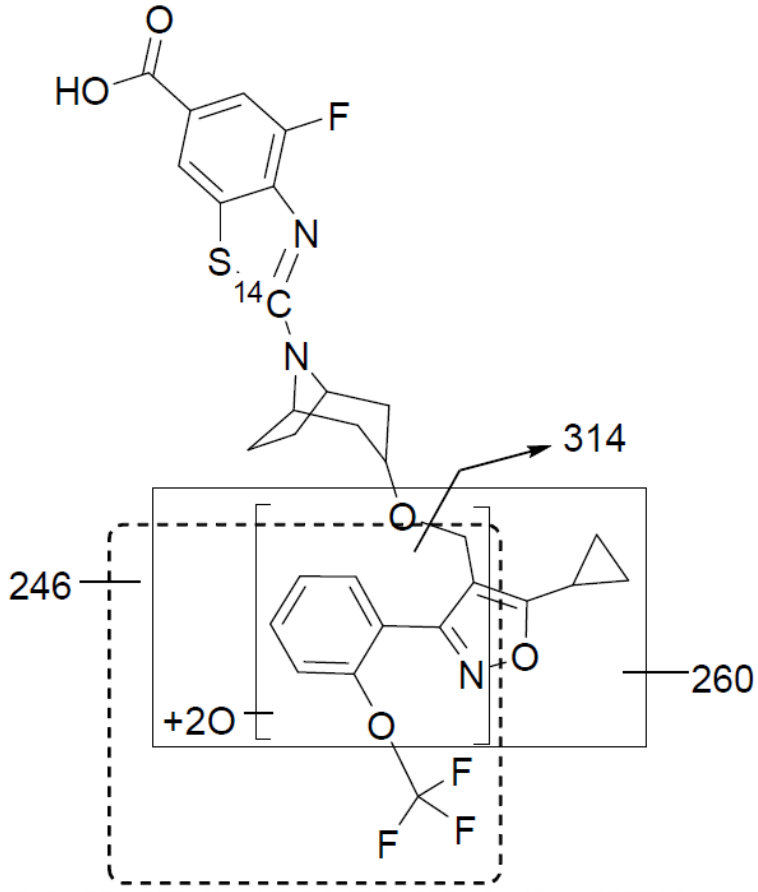

DMD Fast Forward. Published on May 5, 2021 as DOI: 10.1124/dmd.120.000349

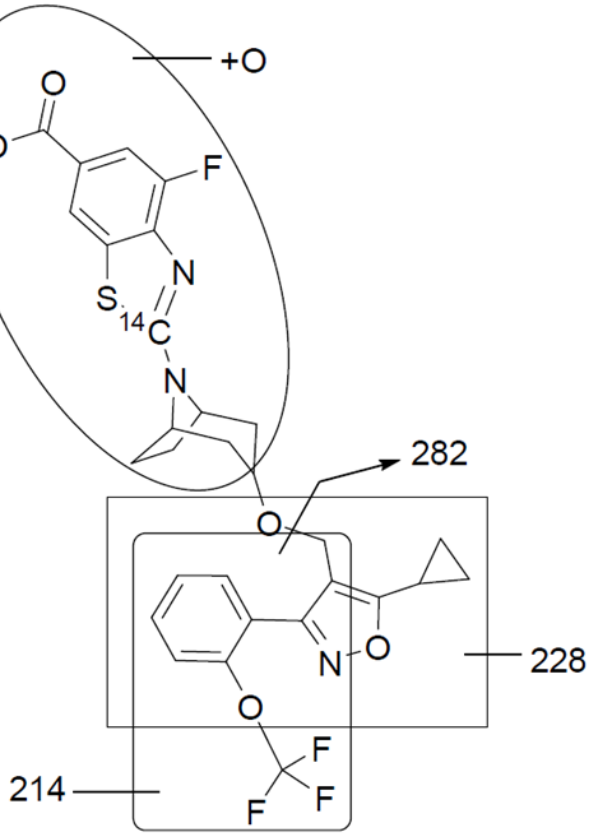

DMD Fast Forward. Published on May 5, 2021 as DOI: 10.1124/dmd.120.000349
This article has not been copyedited and formatted. The final version may differ from this version.

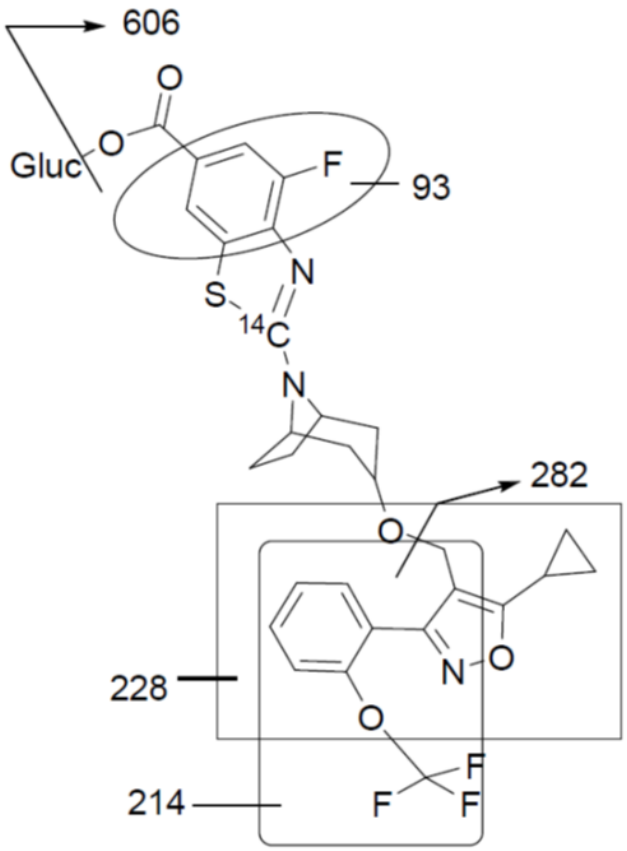

DMD Fast Forward. Published on May 5, 2021 as DOI: 10.1124/dmd.120.000349
This article has not been copyedited and formatted. The final version may differ from this version.

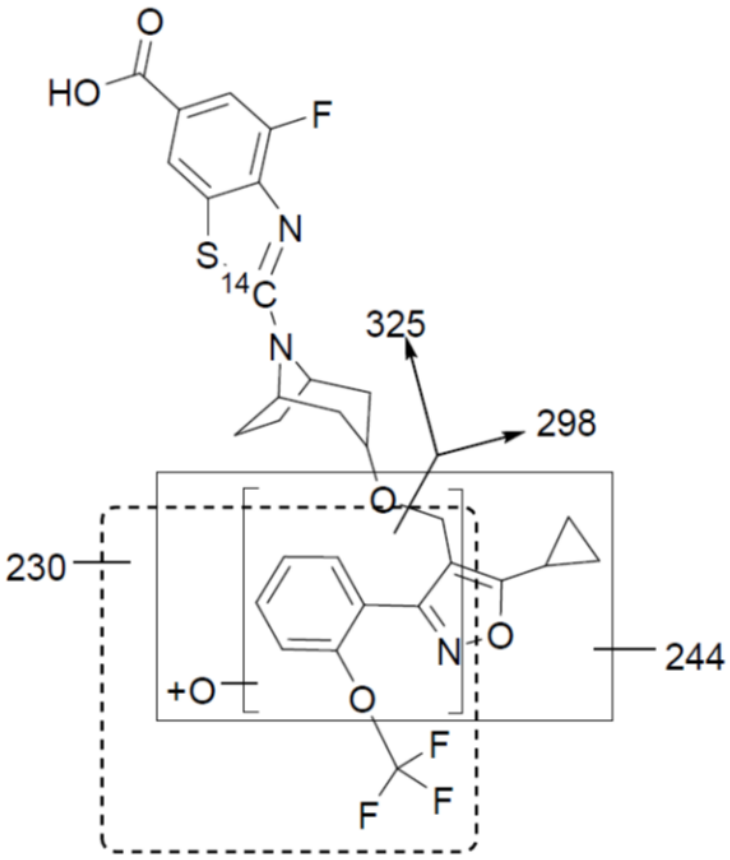

DMD Fast Forward. Published on May 5, 2021 as DOI: 10.1124/dmd.120.000349
This article has not been copyedited and formatted. The final version may differ from this version.